MIL-HDBK-787
1APRIL 1988

MILITARY STANDARDIZATION HANDBOOK

NONDESTRUCTIVE TESTING METHODS OF COMPOSITE MATERIALS-ULTRASONICS

NO DELIVERABLE DATA REQUIRED BY THIS DOCUMENT

AREA NDTI

AMSC N/A

DISTRIBUTION STATEMENT A Approved for public release; distribution unlimited.

DEPARTMENT OF DEFENSE
WASHINGTON, D.C. 20301

MIL-HDBK-787
MILITARY HANDBOOK FOR NONDESTRUCTIVE TESTING
METHODS OF COMPOSITE MATERIALS - ULTRASONICS

1. This standardization handbook was developed by the Department of Defense with the assistance of the Army Materials Technology Laboratory, and Professor Steven Serabian of the University of Lowell, Lowell, Massachusetts, in accordance with established procedure. It is approved for use by all Department and Agencies of the Department of Defense.

2. Beneficial comments (recommendations, additions, deletions) and any pertinent data which may be of use in improving this document should be addressed to: Director, US Army Laboratory Command, Materials Technology Laboratory, ATTN: SLCMT-MEE, Watertown, MA 02172-0001 by using the Standardization Document Improvement Proposal (DD Form 1426) appearing at the end of this document or by letter.

FOREWORD

1. This handbook will eventually become a chapter in a larger volume which will probably include the following military handbooks dealing with composite materials.

Nondestructive Testing Methods of Composite Materials -

Ultrasonics, MIL-HDBK-787
Radiography, MIL-HDBK-733
Acoustic Emission, MIL-HDBK-732
Thermography, MIL-HDBK-731

2. It is intended that the new volume serve as a reference in which answers may be found to the more general questions concerning the technical aspects and applications of ultrasonics to composites. As new techniques emerge, they will be incorporated in the volume.

CONTENTS

CONTENTS - Continued

CONTENTS - Continued

CONTENTS - Continued

CONTENTS - Continued

CONTENTS - Continued

1. SCOPE

1.1 General. This document is intended to provide information on using ultrasound to study several types of discontinuities found in various composite materials. The fundamentals of ultrasonics are not included as this type of information is available in MIL-HDBK-728/6.

2. REFERENCED DOCUMENTS

2.1 Government documents.

2.1.1 Specifications, standards, and handbooks. Unless otherwise specified, the following specifications standards, and handbooks of the issue listed in the issue of the Department of Defense Index of Specifications and Standards (DODISS) specified in the solicitation form a part of this standard to the extent specified herein.

STANDARDS

MILITARY

MIL-STD-371 - Glossary of Terms and Definitions For Ultrasonic Testing Procedures

HANDBOOKS

MIL-HDBK-728/6 - Nondestructive Testing

(Copies of specifications, standards, handbooks, drawings, publications, and other Government documents required by contractors in connection wih specific acquisition functions should be obtained from the contracting activity or as directed by the contracting activity.)

2.2 Other publications. The following document(s) form a part of this standard to the extent specified herein. The issues of the documents which are indicated as DOD adopted shall be the issue listed in the issue of the DODISS specified in the solicitation. The issues of documents whick have not been adopted shall be those in effect on the date of the cited DODISS.

2.2.1 Technical articles referenced in this handbook are listed at the end of this handbook.

(Non-Government standards are generally available for reference from libraries. They are also distributed among technical groups and using Federal agencies.)

3. DEFINITIONS

3.1 Definitions. Definitions given herein shall be as specified in MIL-STD-371, Glossary of Terms and Definitions For Ultrasonic Testing Procedures.

4. COMPOSITE MATERIAL OVERVIEW

4.1 Introduction to composite materials. The use of composite materials is quite extensive. Early military applications generated during World War II have led to large scale commercial applications in such industries as aircraft, aerospace, automotive, boating and sporting industries. The success of fiber reinforced composites is derived from outstanding strength as well as the relative ease of fabrication. Perhaps the one unique characteristic that distinguishes composites from other materials is that the manufacture of a given composite structure and the synthesis of the material occur simultaneously.

4.2 Nature of composites. Some introductory remarks on the nature of composites may be helpful for those unfamiliar with the general subject. A composite material may be broadly defined as one or more discontinuous phases embedded in a continuous phase. The discontinuous phase is much harder and stronger than the continuous phase and is called the reinforcement or reinforcing material. The combination can provide properties not possessed by either of the constituents. For example, one can cite high strength and stiffness to weight ratios compared to more conventional engineering materials such as steel and aluminum. See figure 1 which displays some of the current possible composites. It can be seen that the combination of constituents is unlimited and can include both nonmetals and metals.

4.3. Fiber reinforcements. Reinforcements can be in the form of particles and the composite behaves as an isotropic material. In this paragraph we will discuss continuous fiber reinforcements. Such materials are inherently unidirectional or anisotropic and as such there is a vast difference in mechanical properties in the directions along and transverse to the reinforcements. For example, the strength and stiffness parallel to the fibers in a unidirectional composite may be 25 times greater than the corresponding property measured transverse to the fibers. However, by laminating layers of unidirectional fiber-reinforced materials oriented at appropriate angles one can control the anisotropy for a given design requirement. For convenience uniaxial loadings are usually regarded as acting in the 0° direction and all other fiber orientations are specified relative to this axis. Thus, a $[0, \pm 45^{\circ}]$ material has fibers aligned with the loading direction as well as fibers at $\pm 45^{\circ}$ to the load. The 0° fibers are intended to carry most of the applied stress while the 45° oriented layers contribute to the shear stiffness and off-axis load carrying capacity. The layers of fibers called plies or laminates are arranged symmetrically about the 0° direction to prevent warping. Each laminate must experience the same strain, however the stresses in each layer can be substantially different due to the fact that stiffness depends upon orientation. Thus, the 0° plies are highly stressed while the $\pm 45^{\circ}$ laminates are comparatively lightly loaded. Thus, failure is complex with each oriented layer having a characteristic behavior to an applied stress; this is particularly the case for fatigue failure.

5. FIBER-REINFORCED, ORGANIC MATRIX COMPOSITES

5.1 Use of various fibers. The use of glass fibers is particularly attractive because of the low cost involved. However, graphite, boron and aramid polymer (Kevlar) fibers are highly desirable because of the high strength and stiffness values. There are indications that the price of such fibers will reduce as the demand and manufacturing expertise increase. For example, the price of graphite and boron fibers have decreased during the 1970-1980 period by factors of 10 and 4, respectively.

5.2 Role of the continuous phase. The role of the continuous phase or matrix is to bind the fibers together in a rigid shape, transmit stresses to the fibers and protect them from environmental attack and damage from handling. For the most part thermosetting polymers are used for matrices and include epoxy, polyester, phenolic and polyimide resins.

5.3 Reliability of fiber-reinforced composites. The reliability of fiber-reinforced composites is beset by within - and between-part variability resulting from both raw material variability and the difficulties associated with the control of comparatively new and complex fabrication processes. High strength fibers are often difficult to make with a high degree of uniformity. Alignment of fibers is not always assured; achievement of adhesive coupling between the matrix and fibers can be arduous and many matrix materials evolve gas as an inherent part of the cure process. These variations exist in addition to occasional human error, and one can expect to find anomalies due to:

- o Variations in fiber properties
- o Variations in fiber loading
- o Matrix variations - resin rich/poor areas
- o Variations in fiber/matrix bonding
- o Matrix cracking
- o Porosity (instrand and between layers)
- o Fiber misalignment
- o Gross cracking
- o Breaks in the fibers
- o Gross delaminations
- o Residual stress
- o Foreign inclusions
- o Fabrication parameters - time, temperature, pressure

5.4 Failure. Failure can occur due to any or a combination of the above as they are influenced by exposure to a given operational environment. Any failure can be traced to either the presence of a discrete anomaly or to a deficiency in a particular material property. Unfortunately, the application of nondestructive evaluation methods to composite materials is not well established. Certainly, some of the more gross discrete anomalies involving cracks, delaminations, voids, inclusions and resin variations can be detected and monitored during the use period of a composite component. However, the differentiation of the other more subtle anomalies has yet to be attained. In addition, how most of these anomalies react in a multiple ply structure is not totally understood. Therefore, there is an interpretation problem as well. This is an area where nondestructive evaluation can play an important role in advancing the understanding of composite material mechanics and analysis.

6. INTERROGATION TECHNIQUES

6.1 General. For ease and speed of scanning most interrogations involving flaw detection of composite materials are performed in the immersion mode and the data is recorded as a C-Scan. The initial categorization of the scanning techniques is determined by the specimen thickness. If the thickness is sufficient to resolve the successive back reflections, then a single transducer can be used as indicated in figure 2(a). The resolution is also influenced by the output frequency spectrum of the transducer and is optimized for broadband transducers. If the specimen is thin, as in the general case, then one must resort to a through transmission scanning technique. Utilization of the necessary two transducers is shown in figure 2(b). Both transducers must be critically aligned and their motion must be synchronized. It has been proposed that the latter transducer alignment requirement may be circumvented by using a metal or glass reflector oriented parallel to the specimen (see figure 2(c)). In figure 2(a), reflection A is indicative of a flaw while in (b) and (c) the lack of reflection (A) determines the presence of a flaw.

6.2 Type of transducer used. In all scanning techniques of figure 2, one usually uses a spherical focused transducer. The optimum lateral resolution is primarily governed by the ratio of the lens to transducer radii. The axial or temporal resolution of the focused radiation is governed by the output frequency content of the transducer. One can question the effectiveness of the scanning technique that uses a reflector under the specimen. It is apparent that the sensitivity of the response is decreased due to the added divergence of the beam in its return path back to the transducer.

6.3 Use of the ultrasonic stress wave factor. The use of the ultrasonic stress wave factor as an interrogation parameter was first suggested by Vary and Lark [1]. As we shall see the factor is essentially a measure of attenuation with the added advantage of only requiring single sided specimen assessibility. Commercial equipment is available for the utilization of this technique, however it has not reached the stature of a routine interrogation method.

6.3.1 Attenuation. For the initial interrogation it is convenient to consider a scanning parameter that is a measure of the attenuation of the specimen and is taken as the transmitted amplitude on reflection A of figure 2. Variations of the transmitted amplitude can be related to the existence of delaminations between the plys of the composite, fiber loading, surface irregularities, internal damage, matrix resin variations, void content as well as scattering from various structural components of the composite.

7. DETERMINATION OF FIBER ORIENTATION

7.1 General. The work of Stone and Clarke (2) typifies the ability of transmitted ultrasound to indicate fiber orientation of a fiber reinforced composite. See figure 3. The material is a carbon fiber reinforced composite and the gray scale C-Scan display of reflection A of figure 2(c) clearly shows the alignment of the fibers. The high attenuation (clear regions) at the borders of each display are due to the fabrication process used.

7.2 Technique for detection. Prakash and Owston (3) have suggested a means of detecting fiber orientation. For the moment consider a unidirectional fiber reinforced material. The basic premise of the techniques is that the material acts as a collimator of ultrasound. When the ultrasonic wave is propagated in a direction at some angle to the fiber direction, the material behaves as a discrete lattice and acts as an attenuator because of processes such as reflection, refraction, dispersion, and mode conversion. This is in contrast to propagation along the fibers which provides ease of propagation due to wave guide effects. Figure 4(a) schematically depicts instrumentation to take advantage of this effect. As the angle α is varied the attenuation is altered to disclose the fiber loading direction. This can be significant information when multiple angled lay-ups are concerned. This is quite noticeable for the [0°, 90°] orientations of figure 4. It can be noted that minimum transmission is observed for a unidirectional fiber structure when $\alpha = 90°$ or when transmission is in a direction transverse to the fiber direction. However, as the more transverse or 90° lay-ups are added, the greater is transmission in the transverse direction.

7.3 Acoustic back scattering technique. Bar-Cohen and Crane (4) used an acoustic back scattering technique to locate the orientation of the fibers in a multiple angled lay-up composite. Figure 5(a) indicates the apparatus used. A 25 MHz, 6.35 mm diameter, wideband transducer focused at 12.7 mm operating in the pulse-echo mode was employed to obtain the necessary high resolution requirements. For a given fixed angle α the transducer is rotated such that $0° \leq \beta \leq 180°$. The maximum amplitude is noted within a small angular range of β with the added condition that the beam is normal to the fiber axis. Figures 5(b) and (c) display the results for a $[0°, \pm 45°, 90°]_S$ and $[0°, -15°, -30°, +45°, -60°, +75°, 90°]_S$ laminates where the subscript indicates a symmetrical distribution of the various plys involved. The materials for this study were a glass/epoxy (Scotch 1002) and a graphite/epoxy (T300 Fiber/5200 Resin). All specimens contained at least 2 to 14 plies depending upon the complexity of the lay-up structure and were fabricated using standard autoclave processes.

7.3.1 Scattering differences between glass and graphite. It was noted that the scattering from the glass/epoxy material was 3 to 5 dB higher than that from the graphite/epoxy material. This is presumably due to the much larger difference in acoustic impedance between the glass and epoxy as compared to that between graphite and epoxy. The attendant acoustic impendances of graphite, glass and epoxy are 6.89, 14.5 and 3.48 x 10^6 gm/cm^2 sec. respectively. Thus, the difference in impedance for glass/epoxy is approximately three times that for graphite/epoxy. The latter along with the fiber size and density were responsible for the added scattering from glass/epoxy over the graphite/epoxy composite. In paragraph 8, we shall consider using the experimental apparatus of figure 5 for detecting porosity.

8. VOID CONTENT DETERMINATIONS

8.1 General. The void content in fiber reinforced composites can essentially be relegated to two types: voids that are aligned along individual fibers and voids that are located between the laminates of a multiple ply composite. If the void content is less than 1.5%, the voids are spherical and have diameters within 5-20 mm. For high void contents, the voids are cylindrical and have a length which is an order of magnitude greater than the diameter. Such voids are further characterized by the fact that they are oriented parallel to the fibers.

8.2 Sources of voids. There appears to be two sources of voids: The first is due to the entrapment of air during impregnation of the fiber reinforcement with resin. It has been observed that a highly viscous resin will penetrate with difficulty and this is further aggravated by poor wettability in that all the air will not be replaced. If one adds to this the unique effects of the resin system used along with the influence of the processing temperature, pressure, and time, then it is possible to note the complexities involved in the generation of voids. It is safe to state that a void-free composite is not possible for all practical purposes.

8.3 Measurement of void content. There are a number of techniques for the measurement of the void content. One can list techniques involving the measurement of density by chemical processes (5) and water absorption (6). Comparison with theoretical density will indicate the void content. The micrographic cut-and-see technique is another method of determining void content. All of the latter techniques are destructive in nature. Nondestructive techniques using ultrasound and radiography are also available. However, required sensitivity essentially eliminates the radiographic technique except in those instances where impregnation of absorbing fillers can be used for sensitivity enhancement (7). An estimate of the error for all of the above techniques for determining void content is $\pm 1/2\%$.

8.3.1 Ultrasonic technique. Bar-Cohen and Crane (4) have proposed an ultrasonic technique for determining void content based upon backscatter. Voids were generated by sprinkling hollow glass microspheres between the 0° and 90° plies of a $[0°, 90°]_{2s}$ glass/epoxy laminate. The porosity gives rise to omnidirectional scattering which may be determined by the experimental apparatus previously displayed in figure 5. The results for the porosity experiments are shown in figure 6. The technique has distinct possibilities of being used as a standard procedure.

8.4 Degradation of mechanical properties. Judd and Wright (8) in their excellent summary paper with 47 references on the general subject of the influence of voids in composites, indicate a number of mechanical properties that degrade as the result of the presence of voids. These properties include interlaminar shear strength, longitudinal and transverse strength and modulus, fatigue resistance and high temperature oxidation resistance. For example, regardless of the resin, type of fiber, or fiber preparation, the interlaminar shear strength decreases by approximately 7% for each 1% void content up to a total void content of at least 4% beyond which the rate of decrease diminishes. Other property degradations are not as extensive. It is interesting to note that impact strength increases with void content. This

is attributed to the formation of an extensive yielding zone which produces greater toughness. Williams et al [32] studied the influence of curing temperature and pressure upon the void content of an 8-ply [0°, +45°, 0°] graphite/epoxy Hercules AS/3501-6 composite. (See paragraph 12.)

8.5 Detection of voids. It is obvious that the voids are much too small to produce an appreciable coherent reflection and thereby cannot fall into the realm of flaw detection. However, advantage can be taken of two monitorable events caused by the presence of voids. First, the voids act as incoherent scattering sites thereby detracting from the traversing ultrasound. This should be observable as an increase in attenuation. The second event is that the void content affects the modulus, hence this should be evident by a decrease in the velocity of propagation. As we have noted in other such instances the attenuation variations can be orders of magnitude greater than the associated velocity differences.

8.6 Experimental data. Stone and Clarke [2] have provided the most significant experimental data on the influence of the void content upon the observed attenuation. They worked with a unidirectional carbon fiber material and transmission was perpendicular to the fibers. Their through-transmission, immersion, total attenuation data are shown as figure 7(a). The data is well behaved and the sensitivity of the attenuation at the higher void contents and frequencies is obvious. It was shown by simple impedance amplitude reflection calculations that the indicated attenuation at zero void content may be attributed to the reflection losses on either surface of the specimen. Experimental observations provided evidence that small voids are due to volatile elements present and as previously mentioned such small size voids (5-20 mm) are associated with void contents less than 1.5%. Above this content, the voids are caused by air entrapment between the laminates, and are flatter and significantly larger than the volatile - induced voids. The dual nature of the void structure suggests two distinct relationships and prompted Stone and Clarke to replot their data as shown in figure 7(b).

8.7 Attenuation vs frequency. It is also possible to generate displays of attenuation vs frequency with the void content as a parameter. The slope of this display would be the exponential dependency of the relationship $\alpha \sim f^n$. This is shown in figure 8(a) where the data is taken from the Stone and Clarke display of figure 7(a). The linear relationship on a log-log plot has the added advantage of a predictable functionality, hence facilitates meaningfull data as well as ease in plotting. In grain scattering in polycrystalline materials the exponent n has been very helpful in defining the scattering mechanism involved. The convergence and apparent common point at zero frequency may be interpreted as the attenuation of void free material and is due to intrinsic attenuation and impedance reflection losses at both surfaces of the specimen. A cross plot of this data generates figure 8(b) which displays the frequency exponent (n) as a function of the void content. Again, for the range of void content considered we have a linear relationship once the intrinsic effect is eliminated by simple extrapolation. It is reasonable to state that the measure of the void content in terms of the frequency exponent is a more averaging determination based upon a predictable linear relationship.

8.7.1 Explanation of data. Martin [9] has attempted to generate an explanation for the experimental data of Stone and Clarke. He assumed that all voids are spherical, of the same size and are homogeneously dispersed

cold crossings during ... the number of positive thresh

throughout the resin matrix. Considering only voids in the matrix greatly simplified calculations of the affect of such voids upon the matrix elastic constants. It was further assumed that each void scatters individually, thus multiple scattering is not involved. For ka >> 1 the attenuation due to voids (α_v) becomes,

$$\alpha_v = \frac{3\gamma}{8\pi a^3} v = \frac{8\pi^4}{3} v g \frac{a^3}{\gamma^4} \qquad (1.)$$

where k is the wave number ($2\pi/\lambda$), v is the void content, a is the void radius, γ is the scattering cross section and g is a function of the shear and longitudinal wave velocities. He modified the scattering cross section (γ) as proposed by Ying and Truell(10) by considering the sound velocities as a function of the void content. It is interesting to note that the functional dependency of the void diameter and wavelength are the same as for the Rayleigh grain scattering (kD >> 1) in polycrystalline metals where the average grain size (D) has been replaced by the void radius.

8.7.1.1 Results. A comparison of Martin's calculated attenuation response for the data display of figure 7 is shown in figure 9 where the attenuation response at zero void content has been eliminated. It should be noted that the 5 MHz and 7 MHz curves are above and below the associated experimental data, respectively. Martin attributes this to two possible sources of error: void content and void size. The former under the best of conditions is ±1/2% while the latter can be particularly significant.

8.8 Use of velocity. The use of velocity to monitor the influence of the presence of voids or porosity upon strength related properties in homogeneous materials is numerous. For example, tensile strength correlations have been established by Ziegler and Gertner for cast iron (11); Lockyer (12) for a particulate resin composite; Serabian (13) for concrete and Brockelman (14) for sintered materials.

8.8.1 Propagation directions. In utilizing the velocity as a means for characterizing fiber reinforced composites, propagation directions perpendicular and parallel to the fiber plane(s) are used. Propagating ultrasound within the fiber plane can provide anisotropic elastic constant measurements. However, dispersive effects can hamper the measurement of velocity and its subsequent interpretation. The propagation perpendicular to the fibers is by far the most suitable for nondestructive interrogation purposes and will be considered in this presentation.

8.8.1.1 Theory of Propagation. In unidirectional fiber reinforced composites the accepted theory of propagation is that due to Musgrave (15) and supposes a hexagonal symmetry. The five elastic constants can be determined experimentally - e.g., by rotating a specimen in an immersion bath, and using a through-transmission measuring technique. Martin(16) and Reynolds and Wilkinson (17) have proposed models for the velocity of propagation. The void content is limited to the matrix. In any model it is necessary to account for the effect of voids upon the elastic constants involved. For this purpose, the former used the work of Hasin (18) while the latter adopted the work of Boucher(19).

8.8.2 Velocity vs void content. The results of Martin's model is shown in figure 10 for glass fiber (a) and carbon fiber (b); the effect of the fiber content is also considered. As to be expected, the longitudinal velocity (V_L) and the shear velocities with polarization perpendicular ($V_{S\perp}$) and parallel ($V_{S\parallel}$) to the fiber plane all decrease with void content. Also, increasing the fiber content increases the velocity at any given void content as well as producing a more pronounced velocity decrease. It must be remembered that since it was assumed that the void content is limited to the matrix, any increase in the fiber content would appropriately limit the void content. Also, the elastic constants of the fiber are much larger than those of the matrix. It is significant to note that from the standpoint of sensitivity, the longitudinal wave velocity is desirable for measuring the void content. There is very little velocity-void content data to confirm Martin's model. For example, for a carbon reinforced material, Stone and Clarke [2] indicate a 6% decrease in the velocity for a void content of 5% while Martin's model indicates an 18% decrease.

9. DETECTION OF DELAMINATIONS

9.1 General. Interply delaminations are perhaps the most straightforward anomalies to detect. Using the scanning technique of figure 2.(a) an indication would be noted between the first interface and first back reflection while in figure 2(b) and (c) a delamination would mean total reflection and hence zero transmission. By proper C-scan procedures one can observe these events to map out the delamination. For example, figure 11 indicates the C-scan detection of a delaminate in a 16 ply carbon epoxy reinforced material. The delamination was simulated by embedding a interply square film patch. Of prime importance is the size of the beam at the detection plane of interest. It is for this reason that highly focused beams are used. According to Jones and Stone(20) this can be accomplished by using a simple diameter stop such as a metal washer in front of a flat or unfocused transducer. The increase in resolution is made at the expense of interrogation power. In effect, this produces a smaller source with an attendant highly divergent beam. Broadband focused transducers (see figure 12), or better still, a conical transducer would be more advantageous. Calibration of an interrogation system's ability to completely detail a given size delamination can be made by the use of flat bottom holes drilled perpendicular to the interrogation surface. For the through-transmission immersion mode it is necessary to consider a taping procedure on the drilled side such that the ultrasound encounters a material/air interface.

9.2 Photographic recording system. Knollman et al (21) suggest the use of a photographic recording system to take advantage of the wide tonal range available. Using the double focused transducers shown in figure 13(a), the receiver modulates a light source to indicate the transmitted ultrasound. The noted variations in the light source would then appropriately expose a photographic emulsion. For example, a totally unbonded delamination would be dark on the resulting photographic image while a totally bonded region would appear light. More than 60 shades of intervening gray scales are available. Figure 13(b) and (c) indicates the difference between conventional C-scan and the photographic process presented above. The delaminations were simulated by interply Teflon film inserts in a 14-ply unidirectional graphite/epoxy composite. A comparison reveals the substantial increased clarity of the delamination of the photographic recording. Also, the various gray shades suggest the presence of voids, thickness variations and fiber loading variations.

Chang et al (22) developed a spectrographic technique to detect and locate delaminations. Essentially, the technique is based upon the resonance effect in that destructive interference occurs when the depth of the delamination is an integral multiple of the half wavelength of the ultrasound. Figure 14 shows their apparatus and data where an area without delaminations is used as a standard. Flat bottom holes of 6, 3 and 1.5 mm diameters were used to simulate delaminations.

The straight line relationship between the points of frequency minima and the attendant order number is indicative of the existence of the interferences phenomenon. As displayed in table 1, it was possible to calculate the depth of the delamination. It is significant to note that the sensitivity of the procedure is sufficient to depth locate a delamination of 1.5 mm in diameter. With such sensitivities, it is possible to note crack-like defects as well. The size of any detected delaminations can be found by standard scanning procedures for composites.

10. MEASUREMENT OF STRENGTH RELATED PROPERTIES

10.1 General. The ultrasonic stress wave factor proposed by Vary and Bowles (23) lends itself to studying strength related properties. The crux of the technique is shown in figure 15. The pulse from the longitudinal wave transmitter reaches the receiver in a complex fashion involving interacting phenomena of reflection, mode conversion at the fiber/matrix interfaces and diffraction of waves generated at anomaly sites such as produced by voids and fiber and matrix microcracking. Typical transducer separation range is 1 to 4 inches. The transmitting transducer operates in the high kHz, to low MHz frequency range while the receiver is a medium KHz, resonant type transducer normally used in acoustic emission work. The transducers are usually clamped on; however, Rodgers (24) describes a commercially available, self-contained, portable equipment line which incorporates a tandem set of free rolling contact transducers that have no couplant requirements. Therefore, the stress wave factor measurements take on the full implications of an interrogation technique.

10.2 Stress wave factor (SWF). The stress wave factor (SWF) is taken as,

$$SWF = GRN \qquad (17.1)$$

where N is the number of cycles above a threshold amplitude, R is the pulse repetition rate and G is the sampling time interval. A modified SWF has been proposed by Williams and Lampert (25) which utilizes a single pulse (N = 1) and sums all the amplitudes of the peaks above a threshold apmplitude, thus in effect $G = \infty$. Rogers (24) worked with the RMS values of the voltage peaks and states that this is insensitive to minor changesin waveform shape and eliminates threshold level effects. The stress wave factor is a valid propagation parameter as long as salient items such as transducer activation, transducer characteristics, system gain and transducer separation are held constant. In actuality, the stress wave factor is a measure of attenuation or the ability of the material to propagate ultrasound. It represents a unique attenuation scheme in that only a single specimen side is required. The latter is a particularly desirable feature for examining thin materials such as composites. When the path of the ultrasound is hampered by anomalies then one can expect the stress wave factor to be affected. Since such anomalies can affect strength related properties, a correlation with the stress wave factor should be evident.

10.2.1 Application of SWF. Vary and Lark (1) describe a study using the stress wave factor to investigate the influence of fiber/resin bonding and fiber orientation. The composite consisted of type AS graphite and PR-288 epoxy resin. Fiber orientations studied were $[0^\circ, 10^\circ, 90^\circ]$, $[0^\circ, \pm 45^\circ]_S$ and $[\pm 45^\circ]_S$. Two different fiber treatments were used: with and without polyvinyl alcohol (PVA) coating. Tabs were attached to each specimen to facilitate tensile loading. Each specimen was scanned by conventional ultrasonic interrogation techniques to eliminate those specimens with serious flaws. Stress wave factor measurements were made at 15 equally spaced points within the gage length of the specimen. Figure 16 indicates the results along with the points of fracture due to tensile loading. It can be seen that fracture occurred at the point of the minimum stress wave factor. The latter was noted regardless of the fiber orientation. It should be noted

that in the case of multiple fractures there were corresponding stress wave minima. Since such ultrasonic measurements were made prior to tensile loading, it is obvious that the failures may be attributed to the initial state of the microstructural anomaly content of the material. It is noteworthy that such anomalies were undetectable by conventional ultrasonic interrogation techniques.

10.2.2 Stress wave factor vs ultimate strength. Figure 17(a) shows the relationship of the stress wave factor and the ultimate strength (σ_{ut}). The correlation appears to be valid regardless of the fiber orientation and preparation. As indicated in figure 17(b) there is also a correlation with σ_{ut}^2/E where E is the modulus. The latter quantity is a measure of the strain energy at the ultimate strength - i.e., if x is the gage length then σ_{ut}^2/Ex has the dimensions of energy per unit volume. The stress wave factor, N_{sw}, is expressed in terms of the maximum value noted for SWF and is related to the stress wave energy dissipated. Also note the fiber fractions (f_f) and specimen thickness (t) have been incorporated in the stress wave factor. The PVA coating, in effect, adds to the original diameter of the fiber (5%), thus by considering the ultrasonic parameter as $N_{sw}(t/f_f)$ the influence of the PVA coating can be separated.

11. DAMAGE DETECTION AND EVALUATION

11.1 General. This paragraph will consider the nondestructive detection and evaluation of damage as generated by static and fatigue cycling and as simulated by drop-weight impacts. The effect of the initial anomaly content as acquired during the composite production processes will also be sought.

11.2 Observing initial damage. The nondestructive observation of the initiation of damage in a multiple layered fiber reinforced composite exposed to a stress environment is beset by difficulties primarily due to the anisotropy involved. Each layer of ply because of its orientation with respect to the applied load will fail with its own unique stress level. In general, both strong and weak directions exist and the weakest plies are responsible for the initiation of damage. It is this damage point that must be noted to alert the engineer that failure has started. Needless to say, the nondestructive evaluation method used must possess a significant sensitivity to the damage mechanisms in effect in order to note the minute amounts of such damage. Also, this is further complicated by the fact the damage is volumetric in that it can be spread throughout the composite.

11.3 Damage due to static and cyclic loading. Hayford and Henneke (26) have used attenuation to study the damage resulting from static and cyclic loading histories and have proposed a model to explain the origin. They worked with a graphite/epoxy composite with stacking sequences of $[0^\circ, \pm 45^\circ, 90^\circ]_s$ and $[0^\circ, 90^\circ, \pm 45]_s$. The specimens were nominally one inch wide by seven inches long with bonded fiberglass end taps for load introduction. During the loading, attenuation was continually monitored. Also, the free edges were examined for damage by a microscope as well as by replication techniques. Figure 18 indicates the results for the $[10^\circ, \pm 45^\circ, 90^\circ]_s$ laminate loaded in simple tension; figure 19 displays the crack formation and the acoustic emission results. The similarity of the general shapes of crack formation and attenuation suggests that they are related.

11.4 Cracking. As to be expected it was found that the 90° plies failed first by transverse cracking at load levels approximately one-third of the ultimate strength of the laminate. The entire laminate does not fail catastrophically, but additional transverse cracks continue to appear up to load levels of approximately two-thirds of the ultimate load. At this load level, the transverse cracks have reached an almost regular saturation spacing. (27) Spacings in the 90° layers of 0.024-0.059 inches (0.6 - 1.4 mm) and 0.023-0.043 inches (0.6 - 1.1 mm) were observed for the $[0^\circ, \pm 45^\circ, 90^\circ]s$ and $[0^\circ, 90^\circ, \pm 45^\circ]_s$ laminates, respectively.

It is proposed that the increasing attenuation with increasing load and crack formation is due to the diffraction or beam spreading of the incident ultrasound by the cracks.(28) In effect, the cracks form a regularly spaced diffraction grating. It is important to note that the number of cracks and hence their spacing depend upon the applied load level. Also, as the loads approach the failure strength of the laminate the crack spacing reaches a characteristic spacing unique to the laminate.

12. FATIGUE DAMAGE

12.1 General. When materials are subjected to cyclic or fatigue loading it is well known that they can fail even though the ultimate static strength has not been exceeded. This is true for metals, plastics and composite materials. Within the service life of a structure such fatigue loads are unavoidable, therefore all design criteria must include fatigue analysis as well as static strength requirements. However, for composites the effects of fatigue and the resulting damage are not as well understood as those pertaining to metals. Well established design criteria are not available and one must consider every new material/structure in its own light. Salkind[29] indicates that the growth of fatigue damage in a metal can be much more abrupt (also see figure 20). It is interesting to note that a larger tolerant and inspection threshold damage size exists for the composite material. It would appear that the propagation of damage is arrested by the internal structure of a composite material (see figure 21). Thus, one would expect more desirable fatigue characteristics for the composite material. This is shown in figure 22 for a number of unidirectional composites and affords a comparison with aluminum. The excellent fatigue characteristics of Kevlar- and boron-epoxy as compared to glass-epoxy and aluminum are evident; the graphite-epoxy composite characteristics are also comparable to Kevlar and boron composites. The higher fatigue resistance of a unidirectional composite may be attributed to the fact that the load is essentially supported by high strength fibers. However, there is a general degradation of fatigue characteristics once an off-angle multiple ply structure is considered. As diagrammically shown in figure 23 in a $[0^\circ, \pm 45^\circ]$ stacking sequence much less of the load is carried by 0° fibers and no fibers are aligned in the load direction for the $[90^\circ, \pm 45^\circ]$ composite.[30]

12.2 Complexity. Due to the various constituent components the fatigue damage in a composite is much more complex than say in a homogeneous material such as a common metal. For example, damage is evident by failures due to combination of fiber-matrix interface, matrix crazing or cracking, fiber breaking and delaminations or separation of the plies. The failure modes are further compounded by the presence of manufacturing defects such as scratches, dents, pitting, porosity, voids and delaminations. Experimenters [31, 32] have also indicated that the heat generated during fatigue can significantly degrade fatigue characteristics. Heat generation is both a consequence of and a contributing factor to fatigue damage. Damage such as delaminations and cracking results in significant local internal friction which generates heat. The heat in turn raises the temperature of the material/structure and reduces its resistance to fatigue. This indicates the feasibility of using thermography as a nondestructive evaluation method to monitor fatigue damage.

12.3 Summary. The above failure modes coalesce to produce a degradation of vital material/structure properties and eventually results in a catastrophic failure. The complex interrelationships of these microscopic and macroscopic failure modes present a challenge of major proportions for the nondestructive mode of evaluation to be able to detect, characterize and monitor fatigue damage. It becomes quite evident that no single physical process can totally define damage; thus, no single nondestructive method can fully depict the material/structure degradation due to fatigue damage. The reader is referred to the literature for the activities in thermography, (33) acoustic emission (34) and radiography. (35)

13. USE OF ULTRASONIC C-SCANS

13.1 General. The ultrasonic C-scan continues to be a major means of monitoring fatigue damage. There are inherent limitations primarily due to surface imperfections which tend to incoherently scatter the ultrasound. Perhaps, the greatest limitation originates from the relatively high intrinsic attenuation of fiber composites. This limits the frequency range, hence the minimum detectable anomaly that can be observed. Also, as to be expected the transducer used can significantly influence the results. For example, figure 24 displays C-scans of a $[90^{\circ}, \pm 45^{\circ}]$ graphite/epoxy composite containing a through hole. The extreme left image was obtained by interrogating with a flat transducer (10 mm - 6.7 MHz) prior to fatigue and shows details of surface imperfections in the outer 45° layers; the lowest attenuation level recorded as 11 dB in 1 dB steps. The next three images were obtained after fatiguing. In the first one the plane transducer was used again with 2dB steps; the next is the same transducer but collimated with a 5 mm washer placed at the end of the transducer and the third scan used a long focal length, 6 mm - 10 MHz transducer. The advantage of the long focal length transducer is evident. It can be seen that considerable cracking occurs in the 90° plies. The final rupture lies across the hole and is accompanied by an extensive amount of delamination which shows up as white areas on the scan. There is also an overall lightening in shade of the C-scan after fatiguing which may be due to progressive damage within the whole body of the composite and may be the result of matrix crazing or due to changes at the fiber/matrix interface. Outside the region of extensive delamination each line on the scan in the 90°plies may be assigned to a crack as verified by sectioning. Occasionally cracks can be seen in the 45° plies. The carbon fibers are approximately 7 to 8 microns in diameter, however diffraction causes a much wider trace on the scan image.

13.2 Examples of C-scans to monitor fatigue damage. Another example where the C-scan can be used to monitor fatigue damage is given by Henneke et al [36] (see figure 25). The specimen consisted of a 0° center-notched ply constrained by 90° plies and was cycled at 100% of the notched strength of the 0° ply unconstrained (unidirectional) laminate. The increase in the damage area is clearly delineated.

13.3 Flaw growth during fatigue. Liber et al (37) investigated flaw growth during fatigue in 16-ply graphite epoxy of two different stacking sequences: $[(0^{\circ}, \pm 45^{\circ}, 90^{\circ})_s]_2$ and $[0_2^{\circ}, \pm 45^{\circ}]_{2s}$. They considered simulated flaws consisting of a circular through hole, an interply embedded film patch, an intraply gap and surface scratches. The specimens complete with these induced flaws are shown in figure 26. Each flaw presents a unique localized stress riser. The circular hole produces a planar sharp stress gradient; the interply embedded film patch produces a through-the-thickness stress gradient; the ply gap produces a dispersed stress gradient; and the surface scratch is responsible for a localized high stress concentration.

13.4 Conditions for fatiguing. The specimens were fatigue cycled in tension-compression at a stress level which depended upon the flaw type and represented from approximately 25 to 50% of the static tensile strength of the

corresponding flawed specimens. The maximum load levels for the $[(0^\circ, \pm 45^\circ, 90^\circ)_s]_2$ and $[0^\circ, \pm 45^\circ]_{2s}$ were 23.3 and 32.4 ksi, respectively. A lifetime of exposure was taken as 127,500 cycles which at a cycling frequency of 3Hz was accomplished in 12 hours.

13.4.1 C-scan technique. Each specimen was ultrasonically interrogated in the C-scan/immersion mode after each half lifetime cycling up to a maximum of four lifetimes. Broadband transducers with center frequencies of 5 and 15 MHz were investigated. The final selection was the 5MHz transducer with a diameter of 1 inch and a focal length of 2.5 inches. Figures 27 and 28 indicate the resulting flaw growth contour maps. There are a number of salient observations that can be made. As to be expected the flaw growth is greater in the $[(0^\circ, \pm 45^\circ, 90)_s]_2$ specimens that in the $[0_2^\circ, \pm 45^\circ]_{2s}$ specimens. The influence of the 90° lay up is the dominating factor in this regard.

13.5 Results. For the drilled hole flawed specimen the initial fatigue damage in the form of delaminations is highly localized at the hole within the first two lifetimes then spreads out to the edges. A possible explanation for this lies in the fact that disbonding of laminates can run along the off-zero fibers to the specimen edges and geometrically reflecting across the specimen again. See figure 29 for disbonding effects along the +45° aligned fibers. It should be stated that most of the damage occurs within the number one band.

13.5.1 Results with film patch flaw. In the specimen with a film patch flaw it is apparent that initial delaminations are present throughout the specimen, others are formed with cycling to produce a general growth pattern. In the $[0^\circ, \pm 45^\circ]_{2s}$ specimen with the internal ply gap the damage was minimal and very much confined to the gap area, however with the $[(0^\circ, \pm 45^\circ, 90^\circ)_s]_2$ specimen the damage was throughout. Of the two specimens that contained the surface scratches, the $[0_2^\circ, +45^\circ]_{2s}$ lay-up failed during the first half lifetime of loading. The other scratched specimen showed a growth of delaminations clustered about the horizontal scratch where the surface 0° aligned fibers had been broken.

13.5.2 Residual tensile strength. No significant reduction in residual tensile strength (less than 10%) was observed for any of this group of specimens. This may be due to the relatively low maximum fatigue load used during cycling (from 25-50% of the static strength of the corresponding initially flawed specimens) resulting mostly in noncritical delamination flaw growth.

14. USE OF ATTENUATION

14.1 General. The use of attenuation to monitor the accumulative effects of fatigue damage in homogeneous materials may be traced to Truell and Hikata.[38] Touchert and Hsu[39] in one of the initial papers of such activities in composites indicated that the attenuation increased as a result of fatigue cycling in a glass/epoxy composite (Scotchply type 1002) in both unidirectional and 90° cross plied specimens. Their results are shown in figure 30. Although only a small number of cycles were administered, it can be seen that the attenuation decreases with the unloading of the specimen, however the attenuation gradually increased with the number of stress cycles applied. The attenuation was taken as the ratio of the transmitted amplitude with and without the applied stress, thus the indicated attentuation is actually representative of the increase in attenuation rather than an absolute measurement. It was concluded that attenuation can monitor and quantify the accumulative effects of fatigue damage.

14.2 Correlation between attenuation and fatigue life. Williams and Doll[40] have studied the ability of attenuation to note the fatigue life of a 72-ply unidirectional fiber epoxy composite. They used compression-compression stress cyucling (30 Hz) in a direction within the plies and perpendicular to the fiber direction. The attenuation of the ultrasound in a direction perpendicular to the laminate planes was measured at a variety of frequencies (0.5-2.0 MHz) while subjecting the specimens to maximum stress levels of $0.2\sigma_f$, $0.4\sigma_f$, $0.6\sigma_f$ and $0.8\sigma_f$ where σ_f is the prefatigue static compressive fracture stress. The initial attenuation was found to be the significant attenuation parameter and $0.8\sigma_f$ - 2.0 MHz fatigue data to be the most sensitive. As shown in figure 31 the higher initial attenuation specimens failed during static preload or before the dynamic load had reached its steady state value. It is apparent that there is a distinct correlation between the initial attenuation and the fatigue life.

14.3 Void content on fatigue life. In a later study using the same composite Williams et al [41] studied the influence of the void content upon the fatigue life. Variations in the void content were obtained by altering the cure temperature and pressure. See figure 32. The resulting void content-initial attenuation is shown in figure 33; the correlation of the initial attenuation-fatigue life is shown as figure 34. It is interesting to note that the attenuation for each specimen remained essentially constant up to approximately 10^4 cycles.

15. IMPACT DAMAGE

15.1 General. Williams and Lampert used both through thickness attenuation and stress wave factor to investigate the ability of ultrasound to detect and evaluate impact damage.(25) The material system was a 10-ply unidirectional Hercules AS/3501-6 graphite fiber epoxy composite and has already been described in paragraph 11. The damage was created by controlled free-falling drop-weights whose impact may be characterized by an impact velocity of 4.0 m/sec and an impact momentum of 1.0kg.m/sec along with negligible rebound of the drop weight.

15.2 Test parameters. Each specimen was drop-weight impacted a total of 5, 10, 20, 40 or 100 times after which the residual static 0° tensile strength was determined. The through thickness attenutation and stress wave factor at these same intervals were determined up to the point of the tensile test. For example, for specimens impacted a total of 40 times, the ultrasonic parameters were measured after 5, 10, 20 and 40 impacts.

15.3 Results. Visual damage, in the form of a slight chalking appearance, was first observed at 20 impacts and after 40 impacts fine matrix cracking began to be noted. Figure 35 gives an indication of the extent of the damage created in terms of the residual tensile strength as a percentage of the 0° virgin tensile strength.

15.4 Typical pulses. Figure 36 displays the (a) input pulse and the received pulses for the (b) virgin material and the (c) 100 impact material as noted during the stress wave factor measurements. It can be noted that the impact damage influences the propagation of the ultrasound between the transducers.

15.5 Determination of impact damage. The ability of the through thickness attenuation and stress wave factor to determine impact damage is shown in figure 37. The stress wave factor technique utilizing single pulse activation with an infinite sampling pulse sampling time was used. The stress wave factor was determined by summing the pulse peaks above a threshold amplitude. Figure 38 confirms the fact that through thickness attenuation and the stress wave factor are related in that they both assess the ability of a given material to propagate ultrasound.

16. ELASTIC CONSTANTS DETERMINATIONS USING ULTRASOUND

16.1 General. Accurate determinations of the elastic constants of fiber reinforced materials are necessary to facilitate the determination of their mechanical properties for design purposes. Also, such determinations are indispensible for the evaluation of theoretical micromechanical models for predicting the macroscopic properties of fiber reinforced laminates given the widely diversified properties of the fibers and the supporting matrix.

16.2 Use of the ultrasonic method. There are classical destructive, mechanical techniques available for elastic constant determinations; however the structural complexities of the laminated fiber reinforced composites often produce uncertainties in interpretations and magnify inaccuracies. An alternate to these classical techniques is the use of the ultrasonic method in which velocity measurements are employed. The method has been used extensively for the determination of the elastic constants of single metallic crystals[42] and to describe the various forms of crystalline anisotropy. The ultrasonic method is now being applied to composite materials with a number of decided advantages. For example, the experimental difficulties associated with load introduction during the classical, destructive techniques is avoided; the same specimen can be used for all determinations and the method requires minimum specimen preparation. In addition, the method is nondestructive; hence is applicable for in situ measurements indicative of material characterization or quality.

16.3 Unidirectional fiber reinforced composites. It becomes quite apparent that the bulk of the work on elastic constant determinations has been confined to unidirectional fiber reinforced composites. If the fibers are uniformly distributed in the plane perpendicular to the fibers the composite is said to be orthotropic and nine elastic constants are required to fully characterize the composite. It the fibers are randomly distributed in the plane perpendicular to the fibers the composite exhibits a transverse isotropic structure and five elastic constants are necessary to describe the anisotropy (see figure 39).

that is important to discuss. This relates to signal durations propagation

17. ELASTIC CONSTANTS FROM VELOCITY MEASUREMENTS

17.1 General. We shall primarily be concerned with the transverse isotropic structure illustrated in figure 40. By measuring the longitudinal velocity along the 1 and 3 directions one can determine the C_{11} and C_{13} elastic constants of the stiffness matrix. The velocity measurement essentially consists of determining the transit time through a known specimen thickness. A velocity measurement of shear waves polarized perpendicular to the fiber axis while traversing along and tranverse to the fiber axes, respectively will yield C_{44} and C_{66}. From the latter, one can also determine C_{12} (see figure 39(b)). The propagation and attendant polarization directions for these determinations are indicated in table 2. Other combinations of propagation and polarization directions can be used. Care must be taken to avoid those combinations that are prone to velocity dispersion. For example Zimmer and Cost [43] indicate that they encountered a doubling of the C_{44} constant when using the 1/3 as compared to the 3/1 propagation/polarization direction combination. It was established that the 1/3 combination produced substantial velocity dispersion, thus exaggerating the transit time through the specimen.

17.2 Determination of C_{13}. The determination of C_{13} necessitates propagating at an angle to the fiber direction. The sensitivity of C_{13} is at a maximum when an angle of 45° is used. It is prudent to consider a variety of such angles in the vicinity of 45° and to select the value at precisely 45°. Multiple angle determinations can also aid in the evaluation of the inherent accuracies of the measurement scheme.

17.3 Difficulties associated with angled propagation directions. The difficulties associated with angled propagation directions is that fiber stiffness constants enter the calculations. The reason for this is due to the fact that the direction of the refracted components do not have particle motions that are either parallel or perpendicular to the propagation direction. Any energy that travels down the fibers is spread transverely as a shear wave because of the strong fiber/matrix bond. See figure 41. In general, these waves are not purely longitudinal or purely shear, but have quasi-longitudinal or quasi-shear forms.[43,44] The velocities for three different possible modes are given by: [45]

$$\rho V_L^2(\theta) = \tfrac{1}{2}\,[(C_{33} + C_{44})\sin^2\theta + (C_{11} + C_{44})\cos^2\theta + \phi(\theta)\,]$$

$$\rho V_{\parallel}^2(\theta) = \tfrac{1}{2}\,[(C_{33} + C_{44})\sin^2\theta + (C_{11} + C_{44})\cos^2\theta + \phi(\theta)\,]$$

$$\rho V_{\perp}^2(\theta) = \tfrac{1}{2}\,(C_{33} + C_{23})\sin^2\theta + C_{44}\cos^2\theta \qquad (1)$$

where V_L is the longitudinal wave velocity and $V_{\parallel}$ and $V_{\perp}$ are the shear wave velocities polarized in and normal to the plane of the fibers and the propagation direction; θ is the angle between the fiber axis and the propagation direction. The function ϕ is given by

$$\phi(\theta) = \Big\{ (C_{33} - C_{44})^2 \sin^4\theta + (C_{11} - C_{44})^2 \cos^4\theta + 2\sin^2\theta\cos^2\theta\,[\,(C_{33} - C_{44}) - (C_{44} - C_{11}) + 2\,(C_{13} + C_{44})^2\,]\Big\}^{1/2} \qquad (2)$$

17.4 Relationship of elastic constants to conventional constants. Once the elastic constants have been determined, one can then relate these to the conventional engineering constants. For example, for the transverse isotropic structure we have,

$$E = \frac{C_{33}(C_{11} + C_{12}) - 2C_{13}^2}{C_{11} + C_{12}}$$

$$E_t = \frac{(C_{11} - C_{12})(C_{11} C_{33} + C_{12} C_{33} - 2C_{13}^2)}{C_{11} C_{33} - C_{13}^2} \qquad (3)$$

$$G = C_{44}$$

$$G_t = C_{66} = \frac{1}{2}(C_{11} - C_{12})$$

$$\nu_{13} = \frac{C_{13}}{C_{11} + C_{12}}$$

Where E and G are Young's (axial) and shear modulii, respectively; E_t and G_t are the transverse Young's and shear modulii, respectively; and ν_{13} is the axial Poisson ratio.

17.5 Summary. Similar results for the orthotropic structure are available in the literature.(46, 47) A greater number of velocity measurements involving a more extensive combination of propagation and polarization directions are necessary.

18. AVAILABLE ULTRASONIC TECHNIQUES

18.1 General. All the proposed necessary velocity measurements can be made by the direct contact method of transducer application.(43,46) The transducers for both the longitudinal and shear generated ultrasound are usually bonded by way of a hard bond such as obtained by phenyl salicilate (salol) or a relatively soft bond as produced by a highly viscous oil or grease. For the angled determinations the specimen cuts must be ground and this limits each specimen to a particular angle measurement. Also, for accurate measurements the effect of the bond must be taken into consideration.

18.1.1 Immersion technique. Using the immersion technique circumvents a great deal of the problems associated with direct bonded transducers from the contact method. Also, as we shall see one can generate both shear and longitudinal waves at a wide spectrum of propagation directions without having to cut the specimens normal to these propagation directions. The immersion technique for longitudinal waves was proposed by Assay et al.(48) They essentially noted the time interval difference between propagation through water and through a specimen interposed between the transmitting and receiving transducers. The ultrasound always impinged normal to the specimen, thus only longitudinal wave velocity could be measured. The velocity is given by

$$V_L = \frac{1}{\frac{1}{V_{Lig}} + \frac{\Delta t}{d}} \qquad (4)$$

where V_{Lig} is the longituginal wave velocity in the liquid, d is the specimen thickness and Δt is the observed difference in the delay time caused by the specimen being inserted in the path of the ultrasound.

18.1.2 Immersion technique to measure longitudinal and shear velocities. Markham(49) extended the above described method tc oblique incidence suchthat both longitudinal and shear velocities could be measured. As indicated in figure 42, refraction within the specimen splits the incident longitudinal wave into longitudinal and shear wave components. It must be stated that enough degrees of motion must be available in the specimen support system such that the plane formed by the incident wave and the specimen normal may be oriented perpendicular to the specimen face. This means that the particle motion of the refracted waves are also in the same plane - i.e., within the plane of figure 42. The refracted angles of the longitudinal (r) and shear (r') waves are given by Snell's law as,

$$\frac{\sin i}{V_{Lig}} = \frac{\sin r}{V_L} = \frac{\sin r'}{V_s} \qquad (5)$$

where i is the incident angle of the ultrasound and V_L and V_s are the longitudinal and shear wave velocities within the specimen, respectively.

The difference in the delay time for the longitudinal wave with and without the specimen in place for an incident angle i is,

$$\Delta t = \frac{d}{V_L \cos r} - d\left(\frac{\cos i + \sin i \tan r}{V_{Lig}}\right) \qquad (6)$$

where the refracted angle r may be expresses as,

$$r = \tan^{-1}\left[\frac{\sin i}{\frac{\Delta t\, V_{Lig}}{d} + \cos i}\right] \qquad (7)$$

Relationships comparable to Equations 6. and 7. may be generated for the refracted shear wave where V_L and r are replaced by V_s and r'.

18.1.3 Procedure for determining velocities of refracted waves. The procedure for determining the velocities of the refracted longitudinal and shear waves is first to measure Δt for a given incident angle. By the use of Equation 7 and its equivalent for shear waves one can then calculate both the refracted angles and finally the velocities within the specimen from Equation 5.

18.1.4 Selection of transducers. The selection of transducers is primarily predicated from the beam diameter and the specimen attenuation. It is obvious that due to attenuation the lower frequencies would be mandatory for the shear wave velocity determinations. It must be mentioned that finite beams rather than rays exist in the experiment indicated in figure 42. This means that the receiving transducer would note the existence of a transmitted beam over an extended area. Therefore, to select the position representative of the true transmitted component, it would be advantageous to limit the sampling or receiving area. Usually this can be done by using s small receiving transducer and/or by limiting the extent of the ultrasound that can reach the receiving transducer. Attempts of the latter method include placing small diameter metallic washers on the transducer face or by taping the outer extremes of the transducers by a felt like material.

the same load increment during the prior loading and the

19. TYPICAL RESULTS

19.1 Results of one study. The work of Dean and Turner[50] is shown in figure 43. The material was a unidirectional carbon reinforced composite which possessed a structure best described as being transverse isotropic. The solid line curves are based upon a theory proposed by Hashin and Rosen.[51] The theory predicts the dependence of composite properties on the individual properties and concentrations of the constituents. The proposed model considers a composite made up of parallel cylindrical units which are composed of a fiber surrounded by a coaxial matrix column. In order to fill all space, the units are allowed to vary in diameter but are assumed to have a constant fiber fraction equal to that of the composite. In this way, the model approximates the random packing arrangement of the transverse isotropic structure. It is obvious that reasonable accuracy was attained for the constants of figure 43(a). However, the C_{13} determinations of figure 43(b) have accuracies that only allowed a best-fit description. These C_{13} determinations were obtained from velocity measurements at 45° to the fiber axis. Such measurements presented the most sensitive direction for C_{13}; however a reasonable accuracy of C_{13} necessitated very accurate velocity measurements and other stiffness components. Kriz and Stinchcomb[52] transformed the elastic constant data of figure 43 into engineering parameters. See figure 44 for typical results. The solid lines represent the upper and lower bounds of a modified theory suggested by Hashin[53]

19.2 Another study. Gieske and Allred[47] also present data similar to Dean's and Turner's of figure 43 while working with boron filament reinforced aluminum with three mutually perpendicular planes of two fold symmetry. Such symmetry is termed orthotropic and requires nine constants.

19.3 Measurement of modulus at any angle to fiber axis. Reynolds and Wilkinson[17] discuss a technique to measure the modulus at any angle to the fiber axis. A circular specimen is used and the time measurement for the velocity determination is along the appropriate diameter in a transmit-receive mode, figure 45(a) displays the longitudinal wave measurements for a unidirectional fiber structure. Figure 45(b) gives the results for a (0° 90°) structure with two different types of loading. In the sandwich type of loading all the layers of a given fiber direction are laid down together. In the interleaved structure each different fiber direction layers are alternated. The indicated theoretical model is due to Musgrave.[15] It is apparent that such displays can verify the existence of properly oriented symmetries within a structure.

20. NOTES

20.1 Subject term (key word) listing.

Nondestructive testing
Ultrasonic testing
Composite testing

TABLE I. Ultrasonic spectral analysis results on graphite/epoxy specimens in figure 14. After Chang et al.[22]

Hole Diameter (mm)	Thickness (mm)	Measured Frequency Period (MHz)	Standard Deviation (%)	Calculated Specimen Thickness (mm)	Velocity of Sound (in km s-')
0(Sound area)	5.26	0.321	2	5.26	3.38
6	2.62	0.630	6	2.64	3.38
3	3.05	0.730	1	2.41	3.38
1.5	2.87	0.794	9	2.69	3.38

TABLE II. Elastic constant measurement for transverse isotropy.

Propagation Direction	Mode	Polarization Direction	Constant Determine
1	L	1	C_{11}
3	L	3	C_{13}
1	S	3	C_{44}
3	S	1	C_{44}
3	S	2	C_{66}

* See figure 40

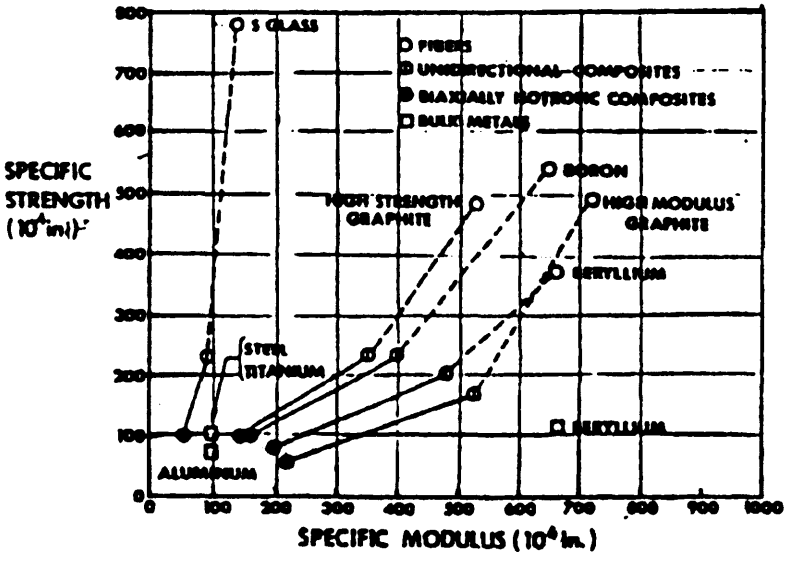

FIGURE 1. Strength and stiffness of advanced composite materials. After Jones[54]

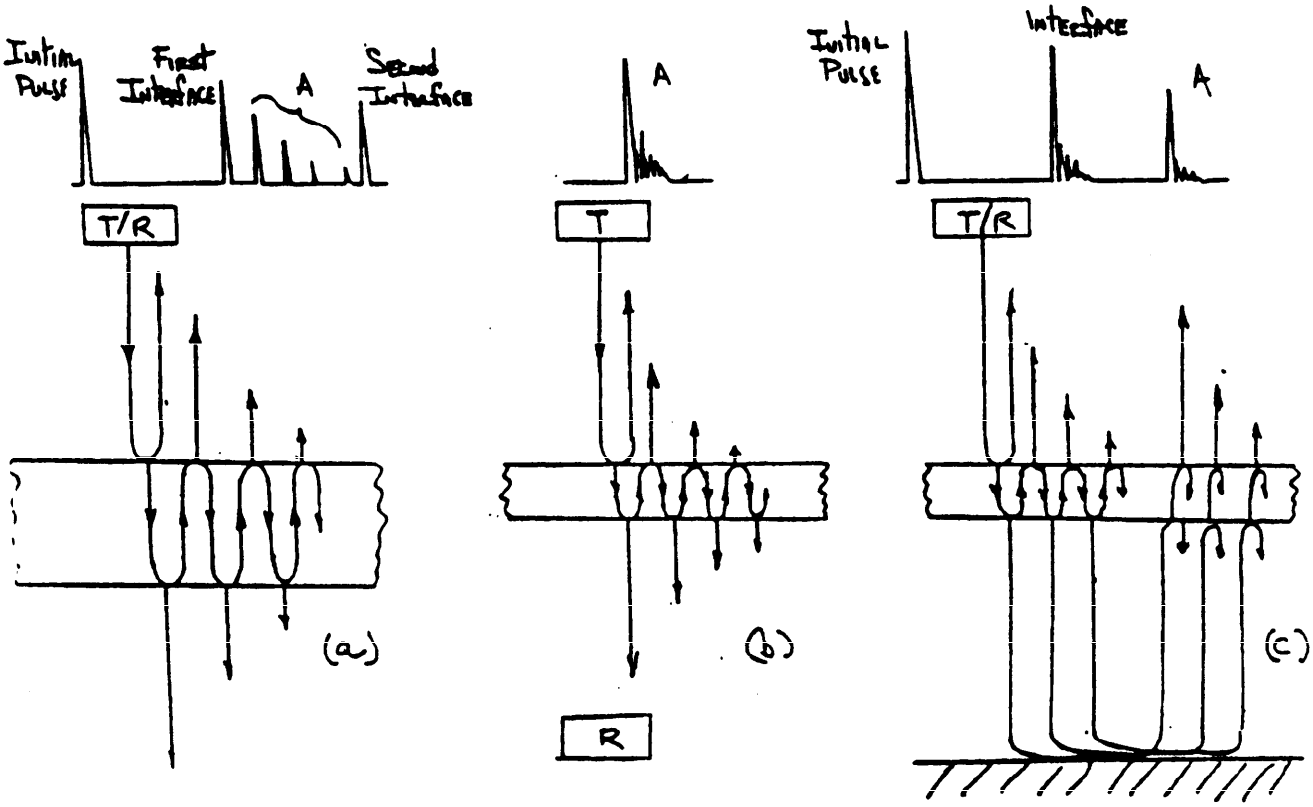

Figure 2. Various immersion scanning techniques. In each case the salient amplitude(s) are indicated with the letter A. For the sake of convenience all reflections have been displaced to the right. In (b) and (c) detracting reverberations within the specimen can be seen.

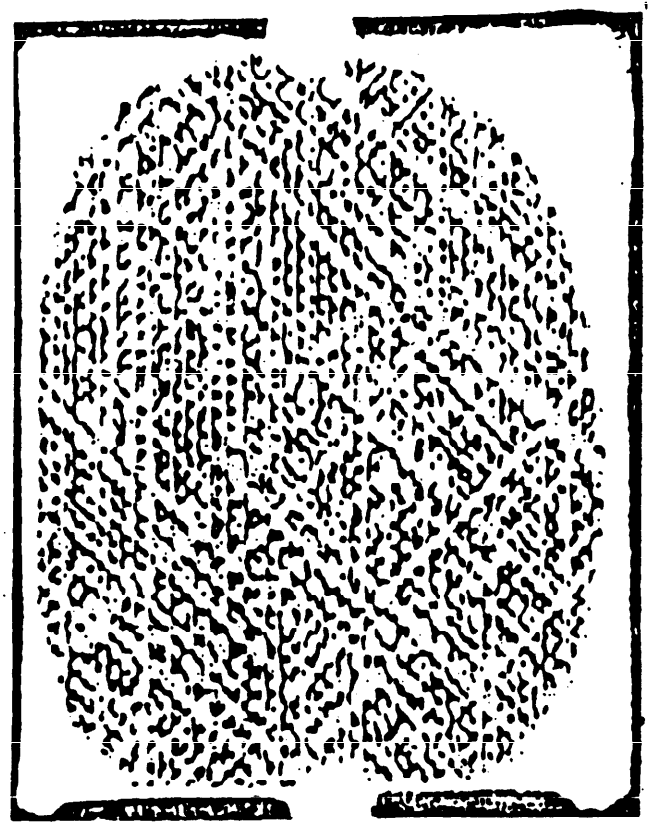

(a) The fiber alignment is $[0^\circ,45^\circ]$ and the specimen is 3mm in thickness

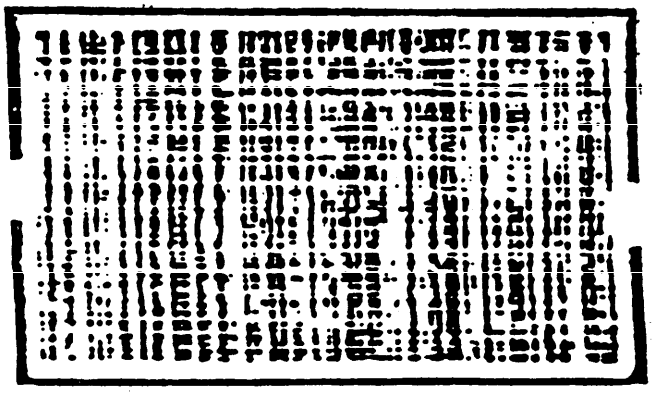

(b) The fiber alignment is $[0^\circ,90^\circ]$ and the specimen is 2mm in thickness

FIGURE 3. C-Scan displays of carbon fiber reinforced composites indicating the fiber alignment. An interrogation frequency of 10 MHz was used. After Stone and Clarke.(2)

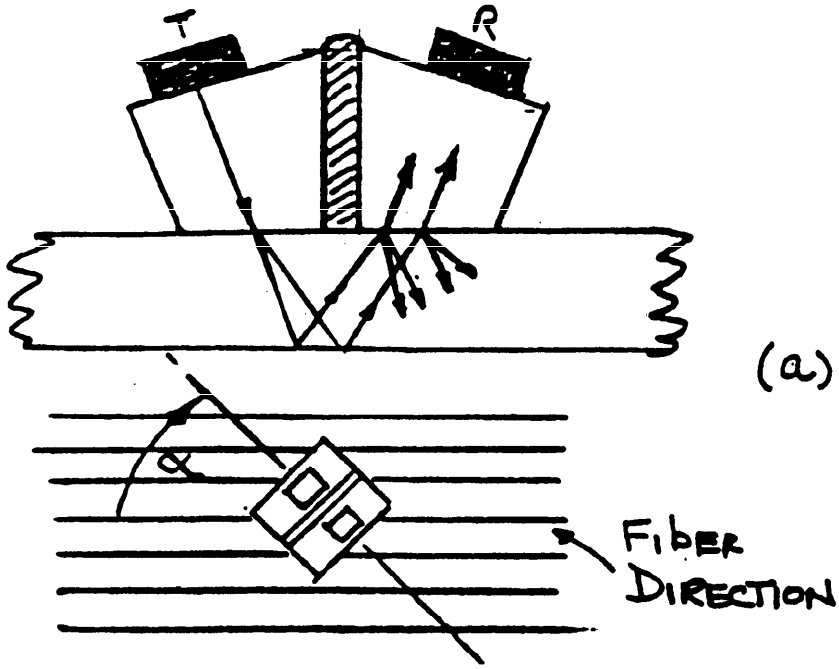

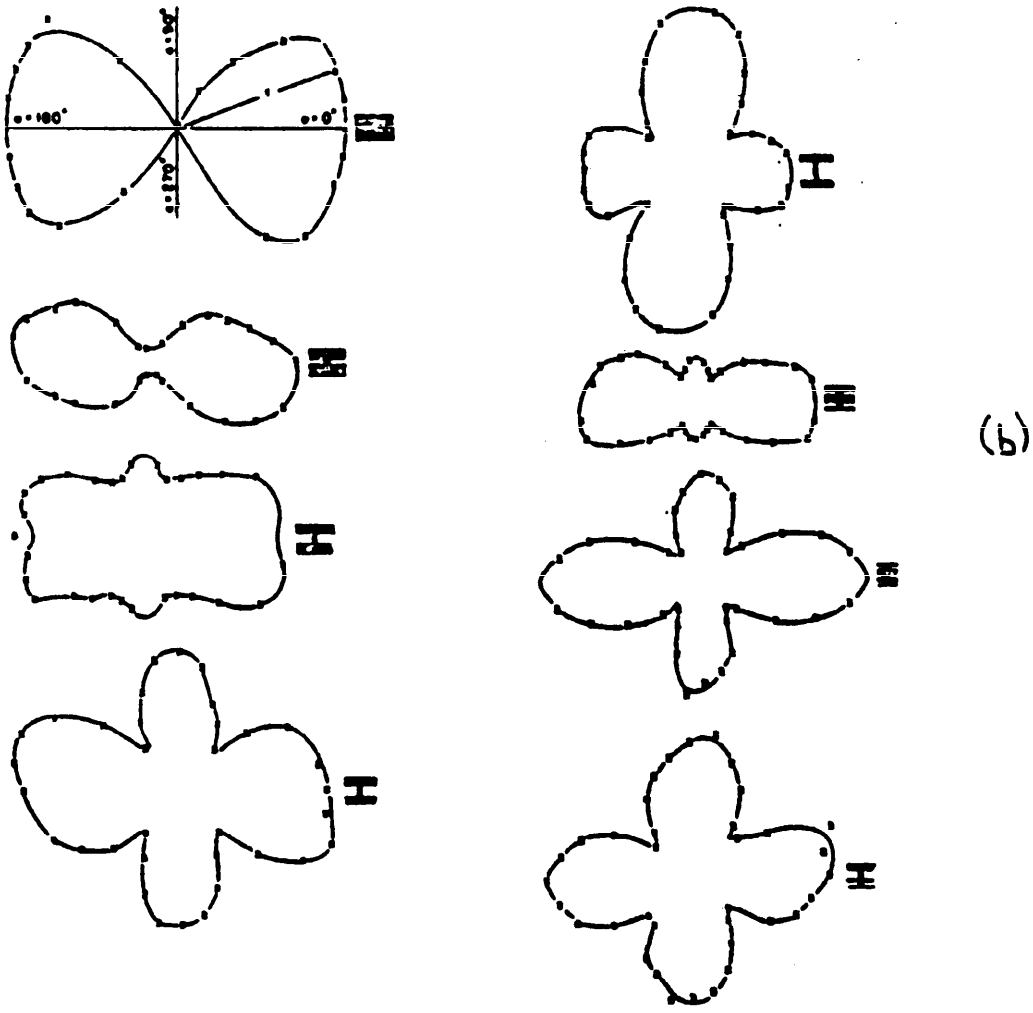

FIGURE 4. Experimental determination of fiber orientation. After Prakash and Oweton[3]

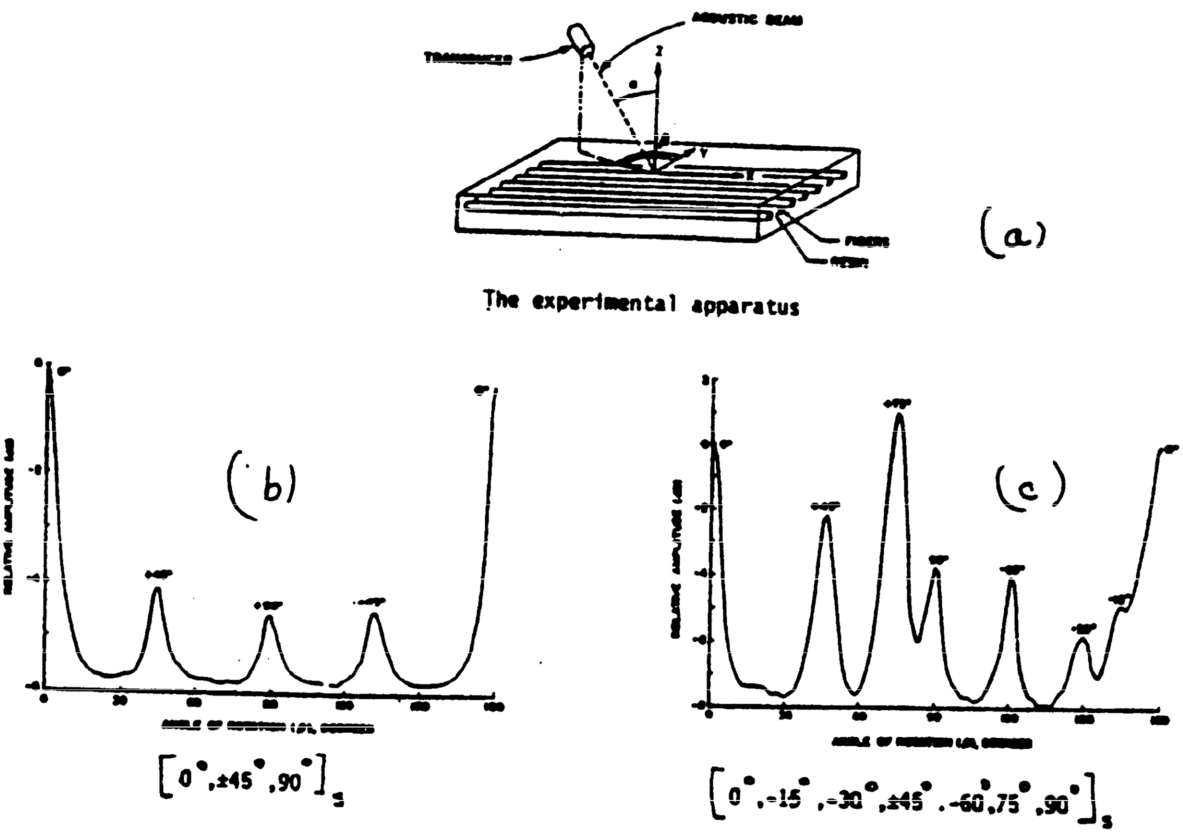

FIGURE 5. Backscattering experiments to locate the fiber direction in a graphite/epoxy composite; $\alpha = 30^{0}$. After Bar-Cohen and Crane.(4)

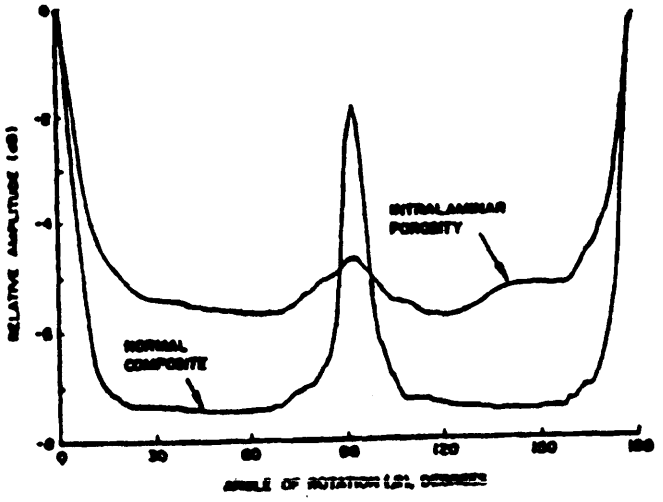

FIGURE 6. Backscattering experiments for a $[0^{\circ}, 90^{\circ}]_{2s}$ glass/epoxy composite with and without interlaminar porosity generated by sprinkling hollow microspheres between the 0° and 90° layers. After Bar-Cohen and Crane.[4]

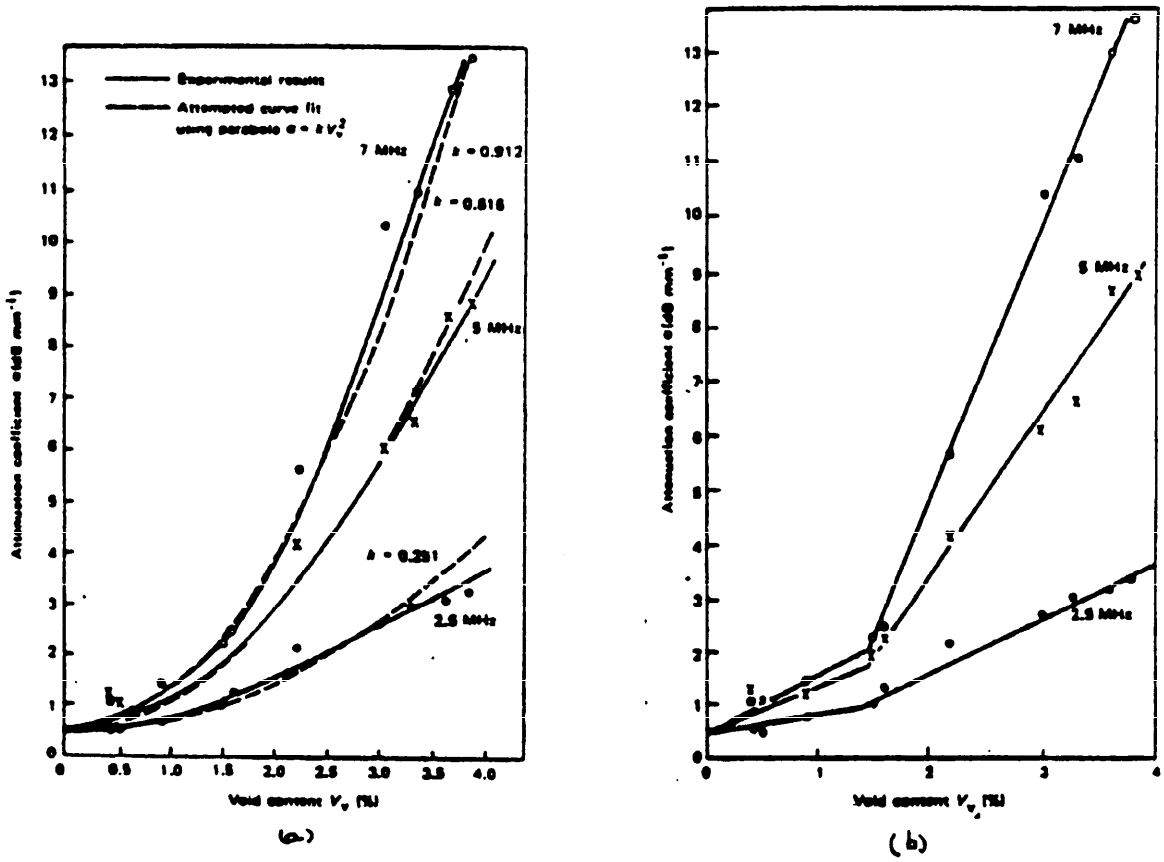

FIGURE 7. The attenuation-void content experimental data of Stone and Clarke.(2)

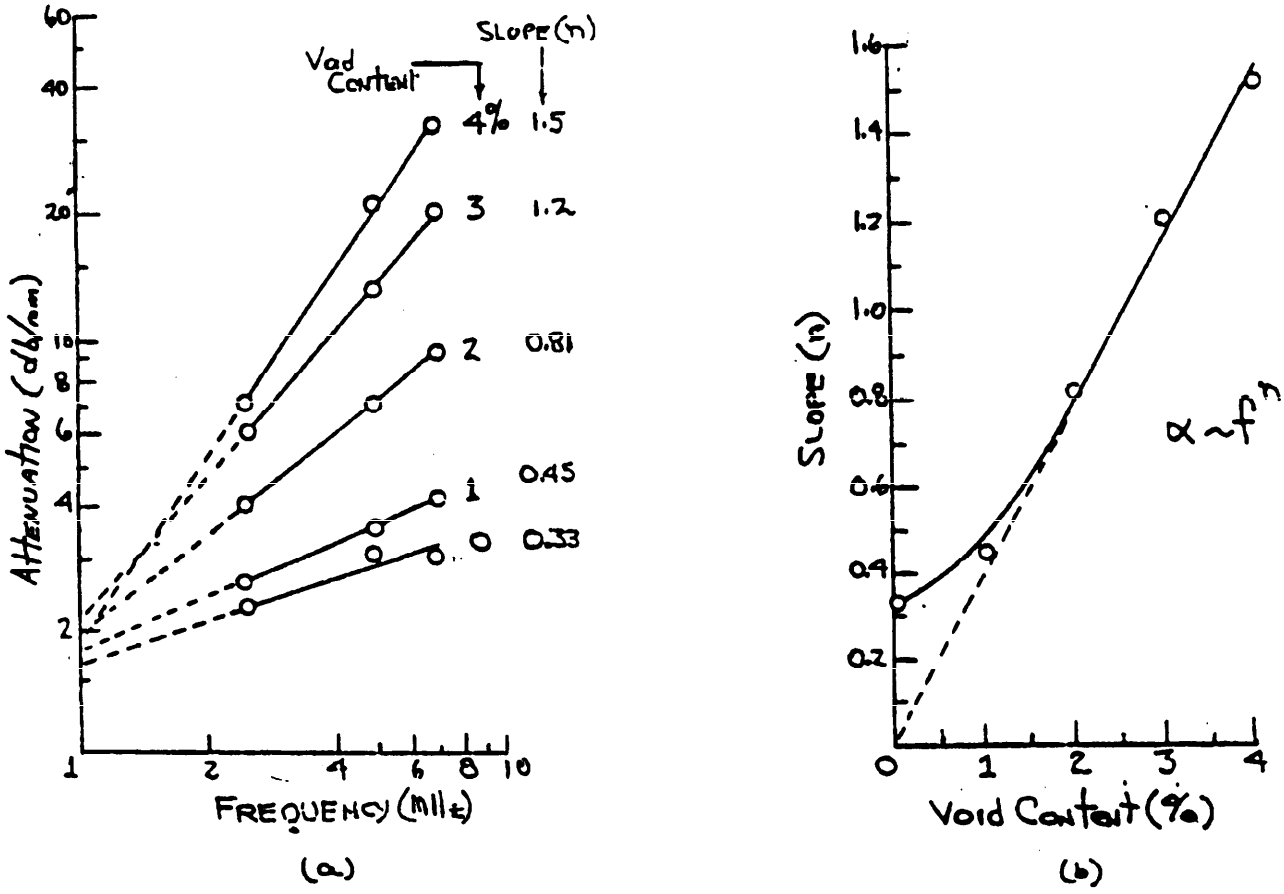

FIGURE 8. Replotting the experimental data of Stone and Clarke (2) to disclose the frequency exponential dependency of attenuation, n, (part a). Part (b) shows n as a funcion of the void content.

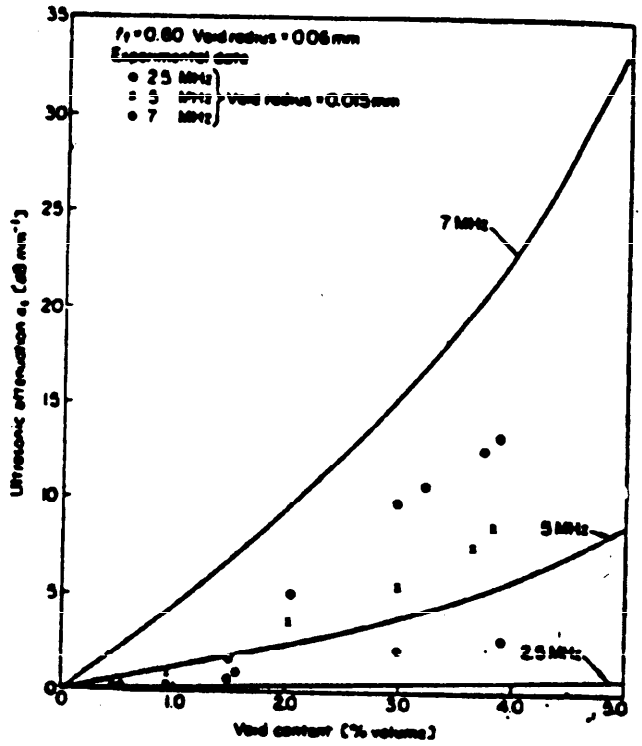

FIGURE 9. Martin's model (9) results compared with the attenuation-void content experimental data of Stone and Clark.(2)

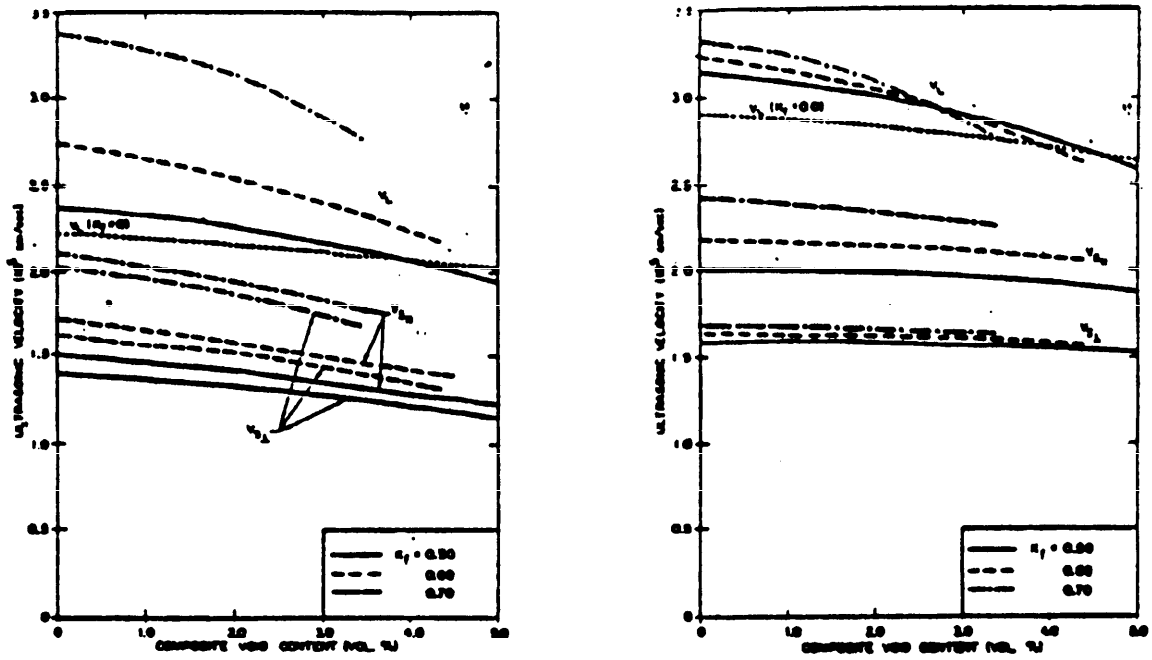

Glass Fiber

Carbon Fiber

FIGURE 10. Ultrasonic velocity as a function of the void content for several values of fiber content (K_f). After Martin (16)

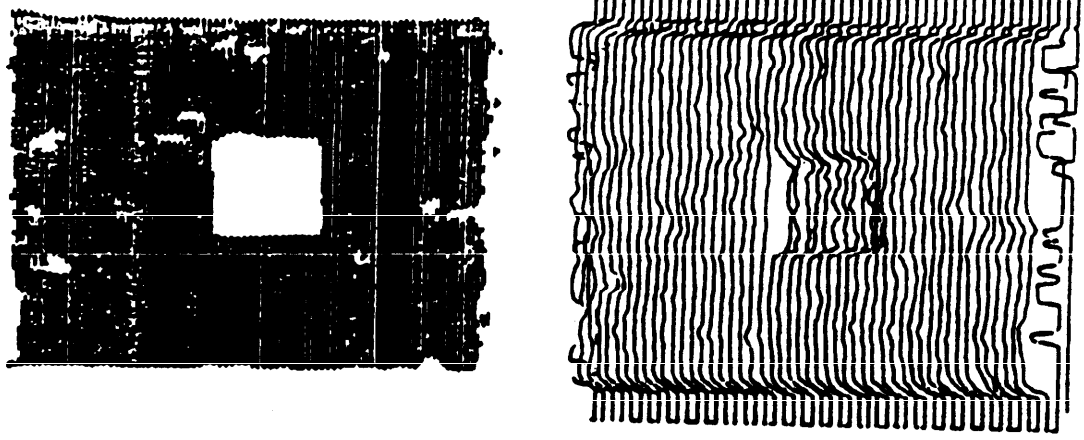

Pen-lift Scan

Analog Scan

FIGURE 11. A delamination in a carbon/epoxy specimen (0 , +45, 90). The delamination was generated by an interply film patch. A 5 MHz focusted transducer with a nominal 2.5" focal length was used; the 0.050" focal spot is indicative of the detection sensitivity. After Liber et al (55).

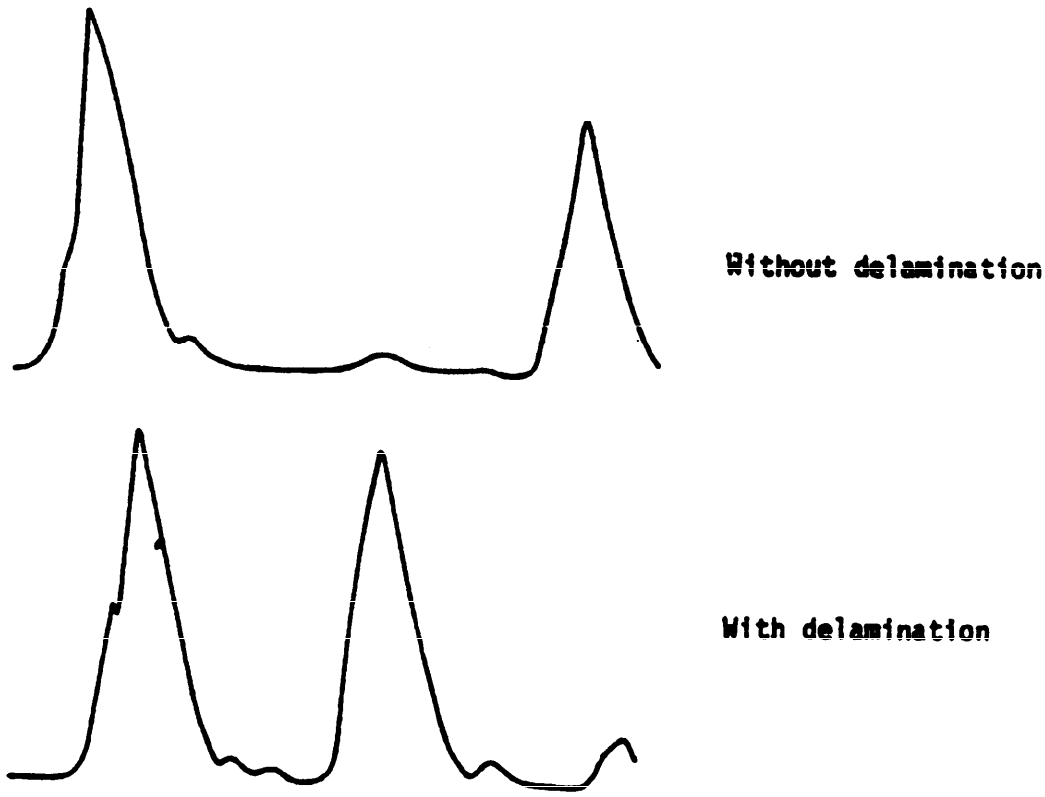

FIGURE 12. The detection of a delamination by the pulse-echo mode of immersion scanning with a sufficiently focused high frequency (10 MHz) transducer. Delaminations 0.25 mm below the surface have been successfully detected. After Stone and Clarke.(2)

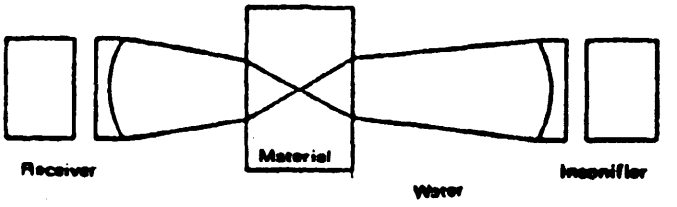

Ultrasonic Apparatus
(a)

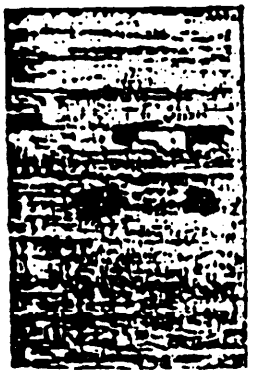

Conventional
C-Scan
(b)

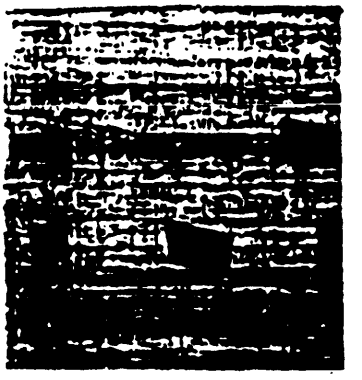

Photographic
Recording
System
(c)

FIGURE 13. This recording technique utilizes the large tonal gray scale of a photographic emulsion. The transmitted ultrasound modulates a light source which in turn produces the images. The image enhancement by the photographic process as compared to the conventional C-Scan is evident. The specimen is a 21-ply unidirectional graphite/epoxy composite; the images are due to delaminations as produced by interply teflon films. After Knollman et al.[21]

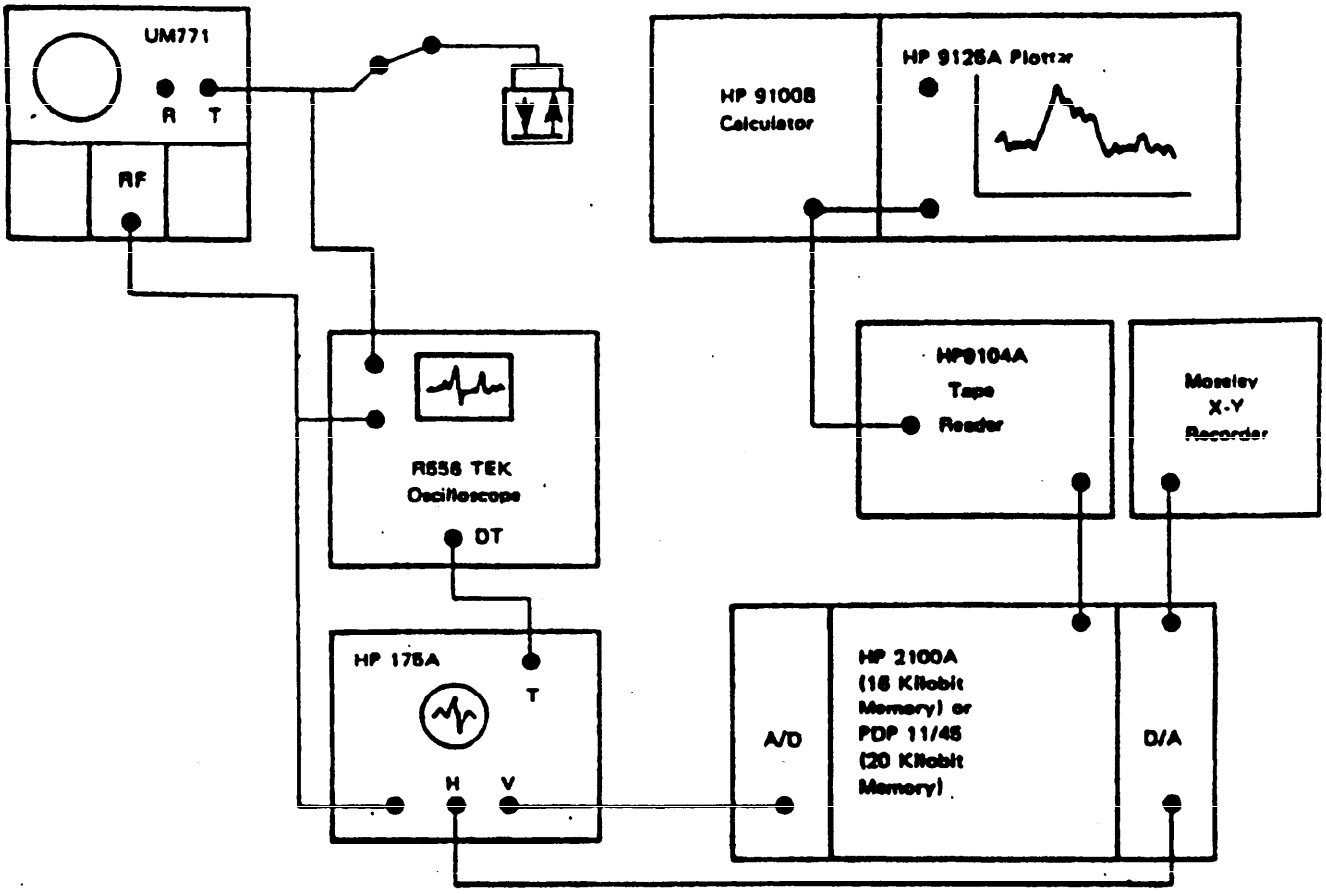

Block diagram of measurement system elements

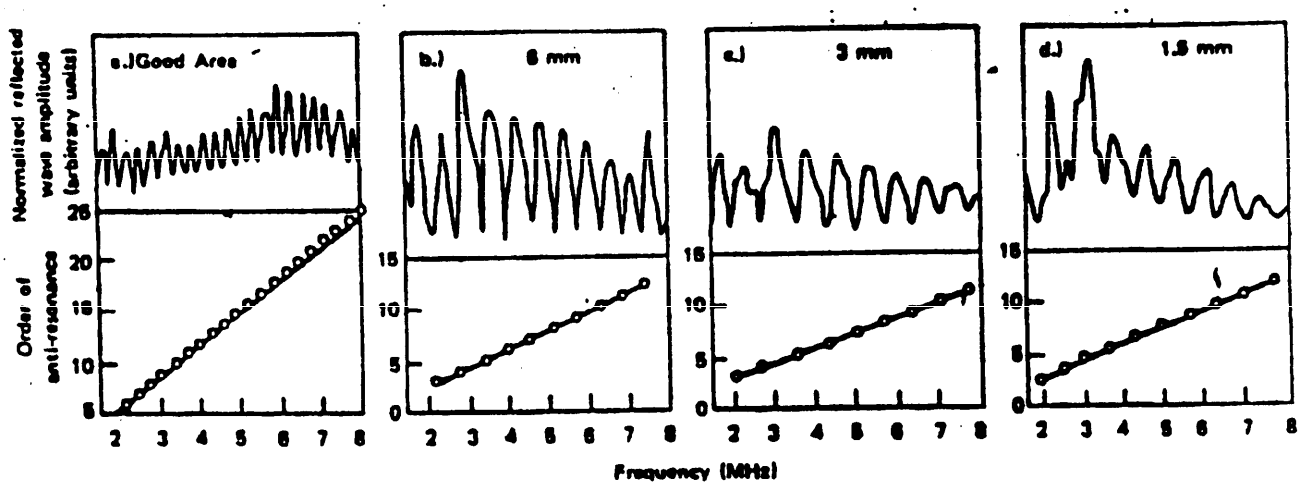

Spectra from delaminations (flat bottom holes)---b,c,d and a good area---a

FIGURE 14. Detection and location of delaminations by spectral analysis. After Chang et al.[22]

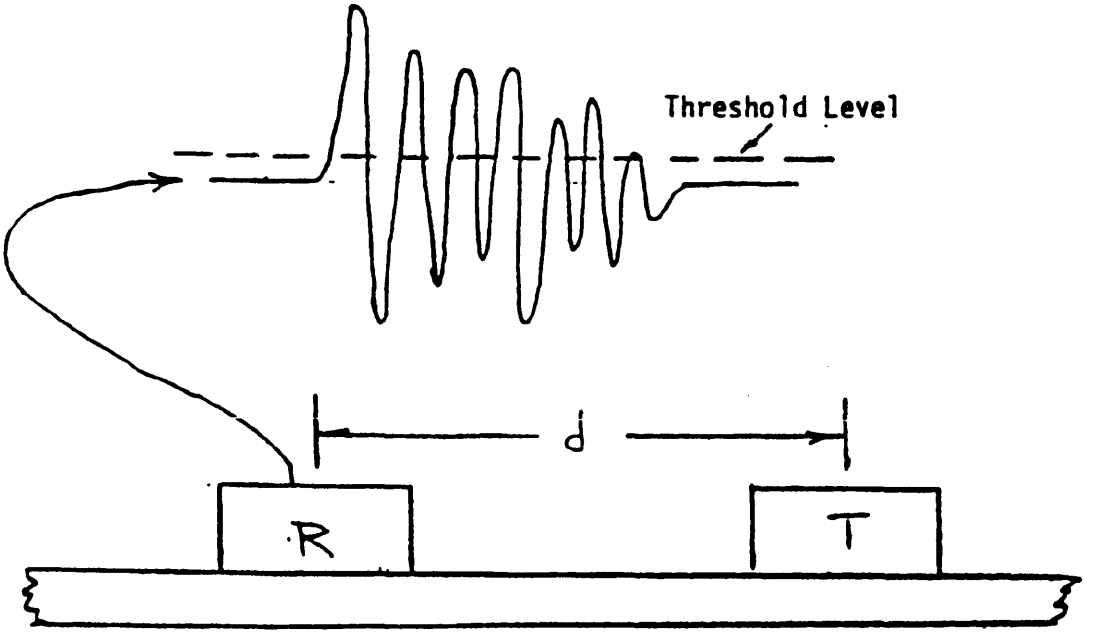

FIGURE 15. The acoustical stress wave factor measurement.

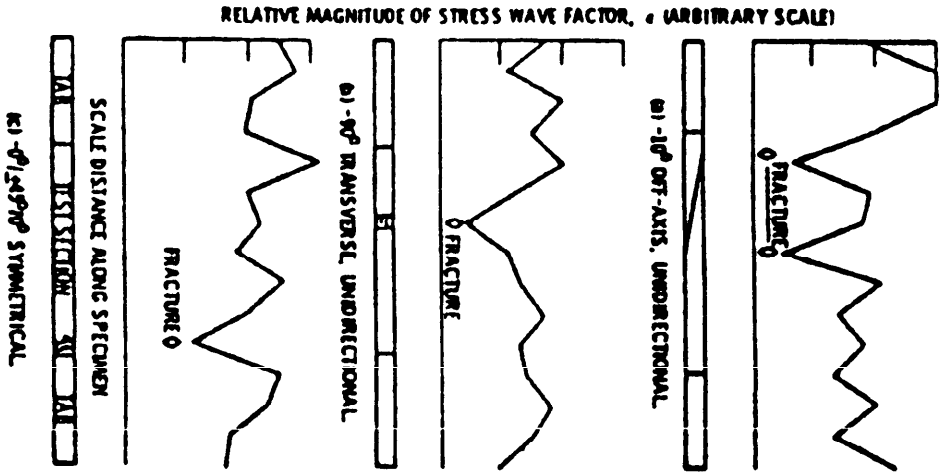

FIGURE 16. Typical variations of the stress wave factor along tensile specimens. Note that fracture occurs at the point of of minimum stress wave factor. After Vary and Lark.(56)

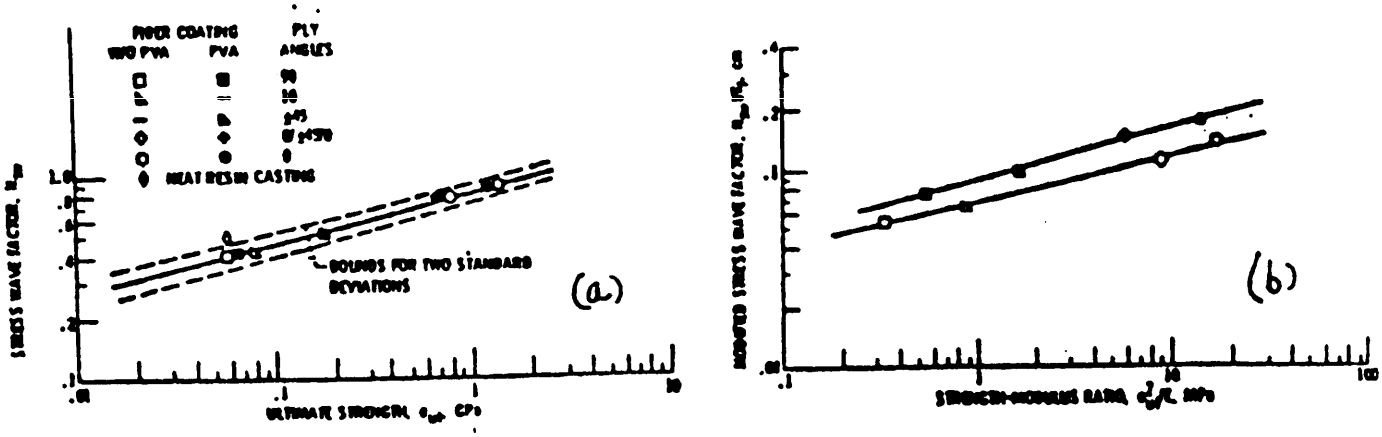

FIGURE 17. Stress wave correlations with (a) ultimate strength and (b) strength-modulus ratio. After Vary and Lark.(1)

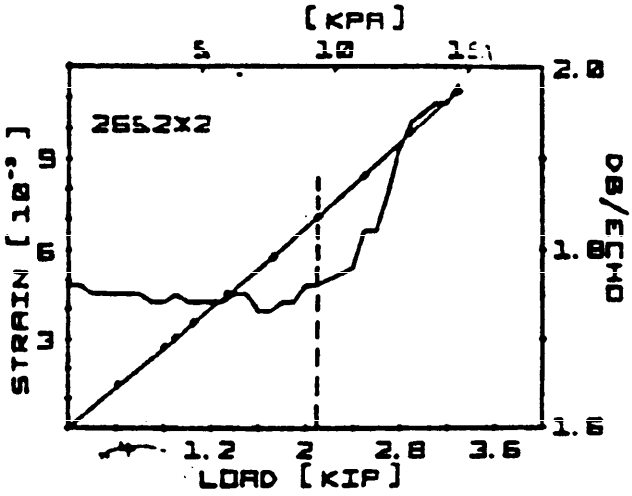

FIGURE 18. Attenuation and stress-strain responses for a graphite/epoxy specimen with a $[0°, +45°, 90°]_s$ stacking sequence. After Hayford and Henneke.(26)

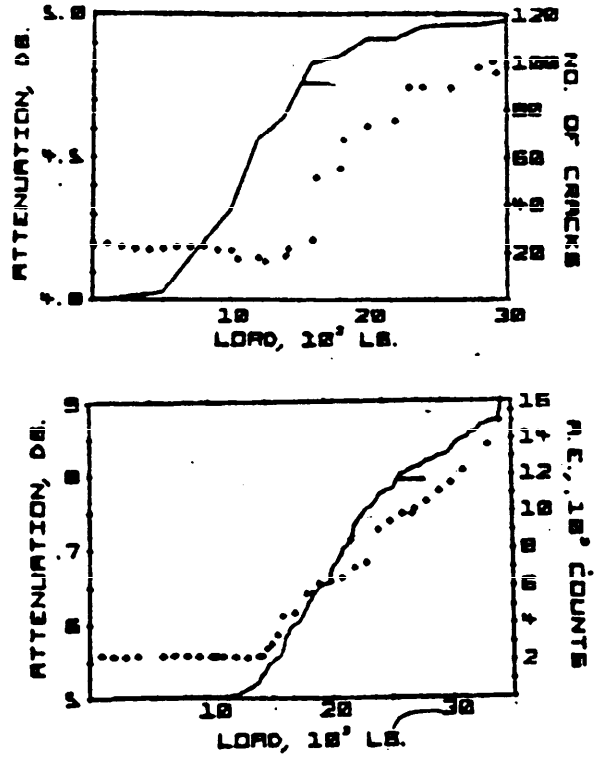

FIGURE 19. Crack formation (a) and acoustic emission (b) with load of a graphite/epoxy specimen with a $[0°, \pm 45°, 90°]_s$ stacking sequence. After Hayford and Henneke.(26)

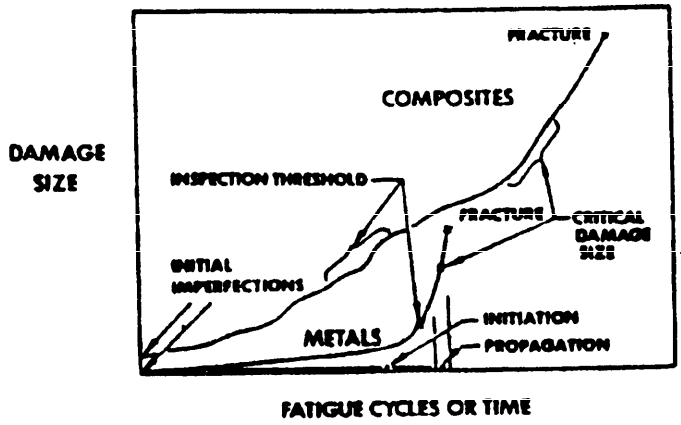

FIGURE 20. Fatigue damage characteristics of typical composites and metals. After Jones.(54)

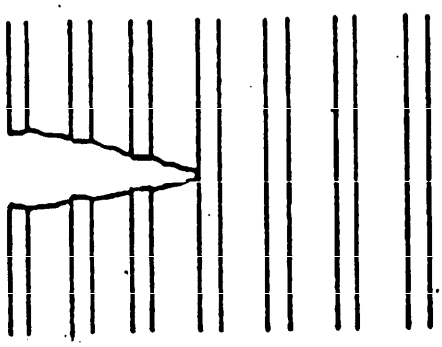

Crack propagation -- Strong fiber/matrix interface bond
(Brittle Fracture)

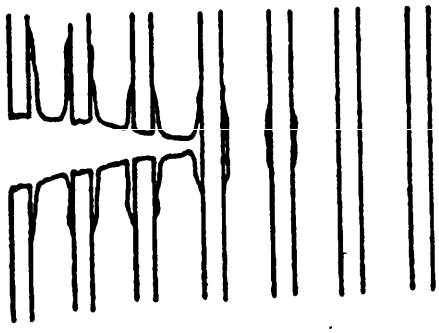

Crack propagation -- weak fiber/matrix interface bond
(crack blunting)

FIGURE 21. The debonding of a weak fiber/matrix interface can absorb energy thus improving toughness. After Sturgeon.(30)

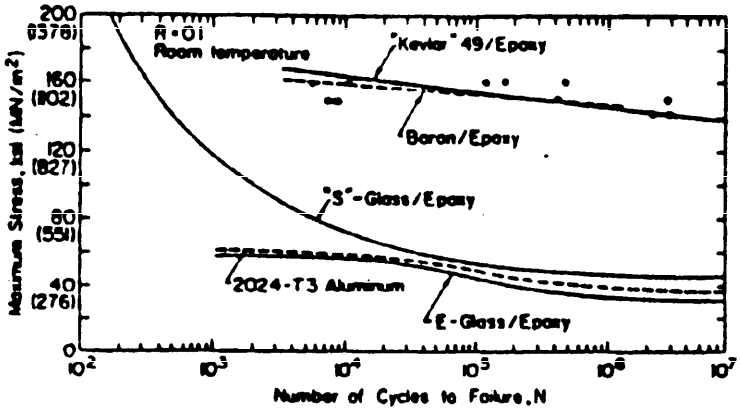

FIGURE 22. Comparison of fatigue characteristics of some unidirectional composites and aluminum. After Agarwal and Broutman.[57]

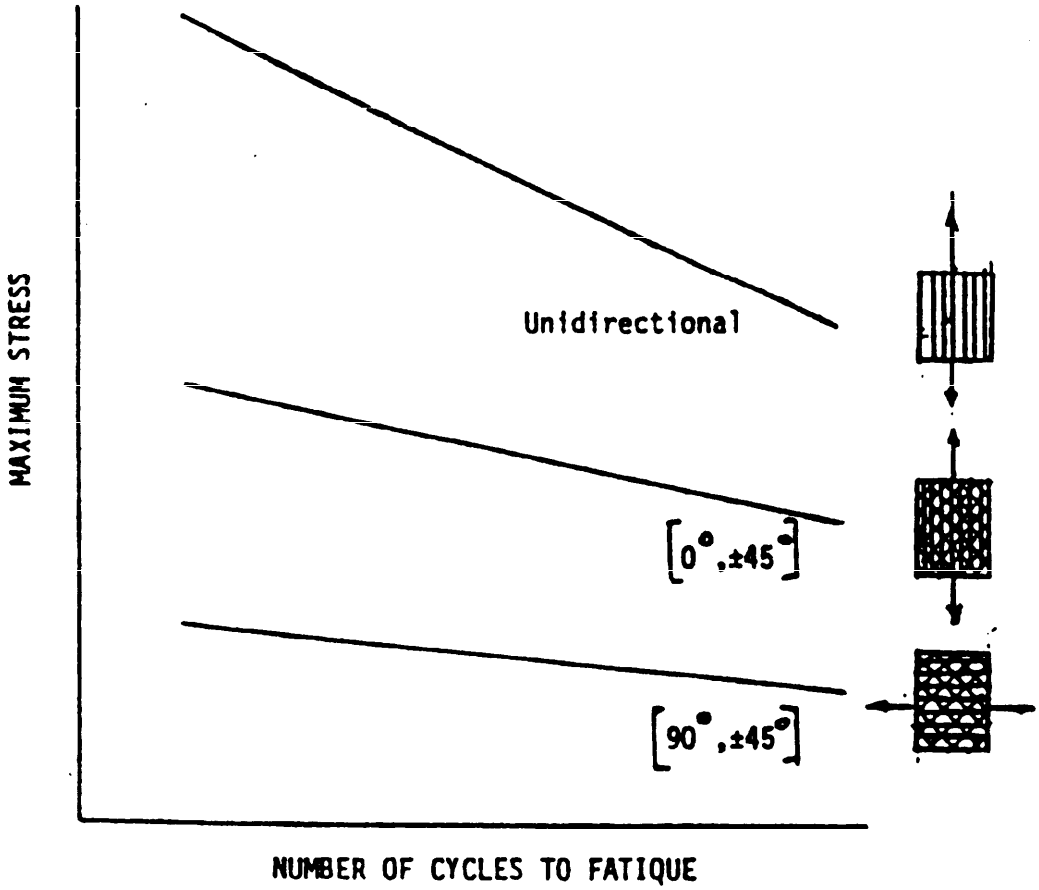

FIGURE 23. Influence of the stacking sequence upon the fatigue characteristics of a fiber reinforced composite.

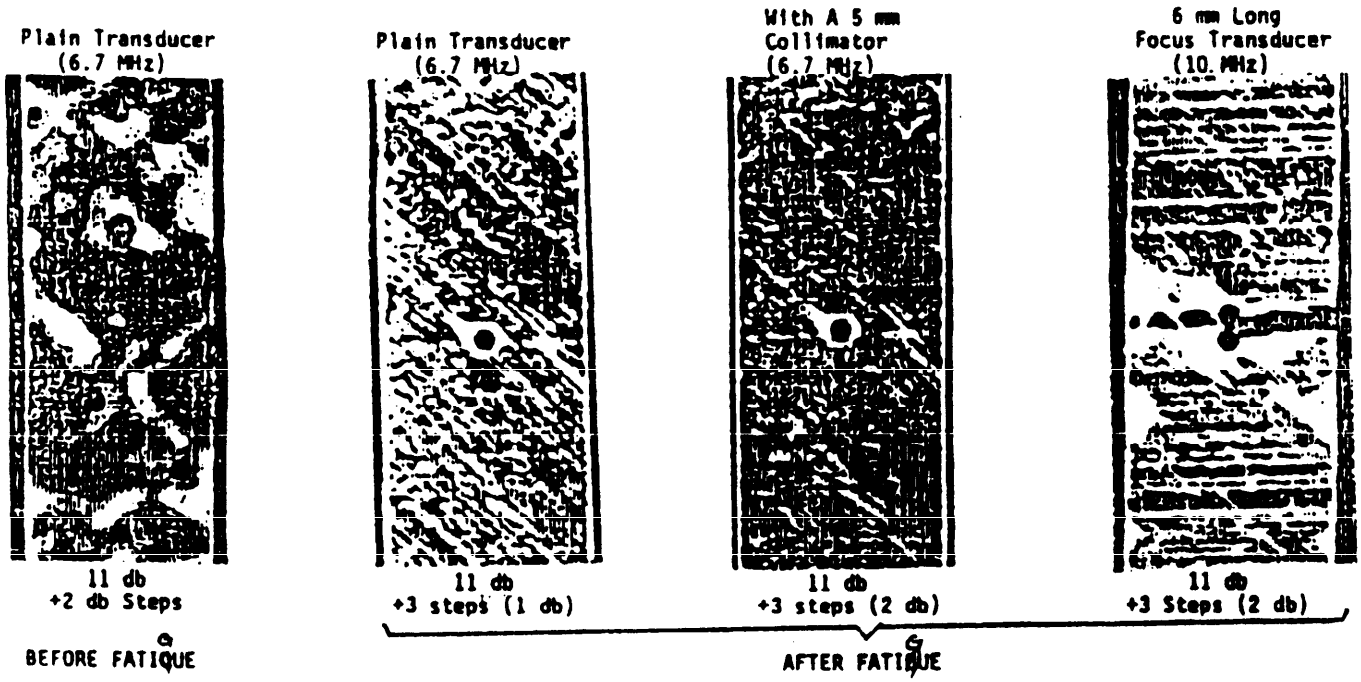

FIGURE 24. The ultrasonic C-Scan monitoring of fatigue damage. After Sturgeon.(30)

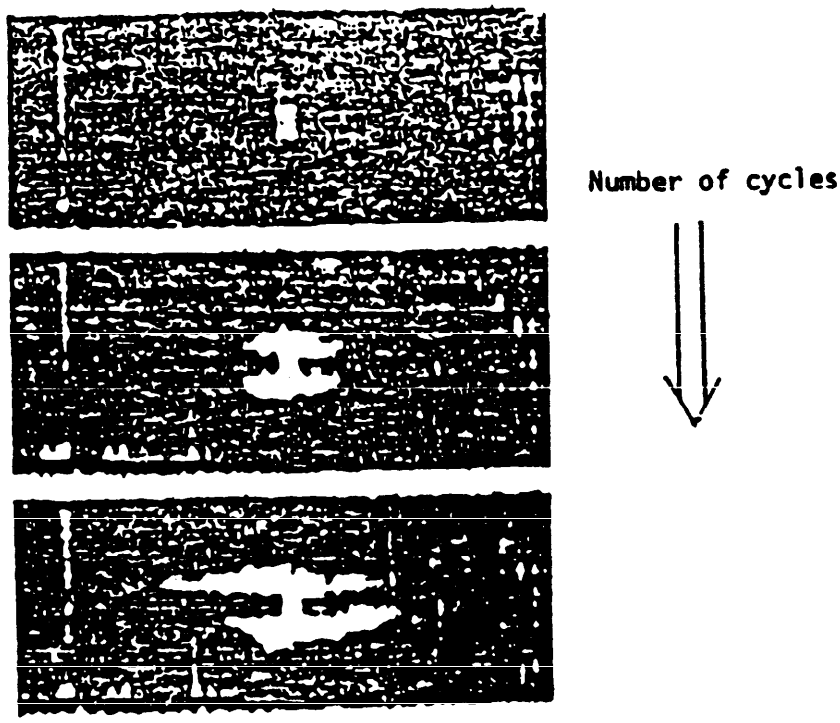

FIGURE 25. Damage growth as noted by an ultrasonic C-Scan interrogation. After Henneke et al.(36)

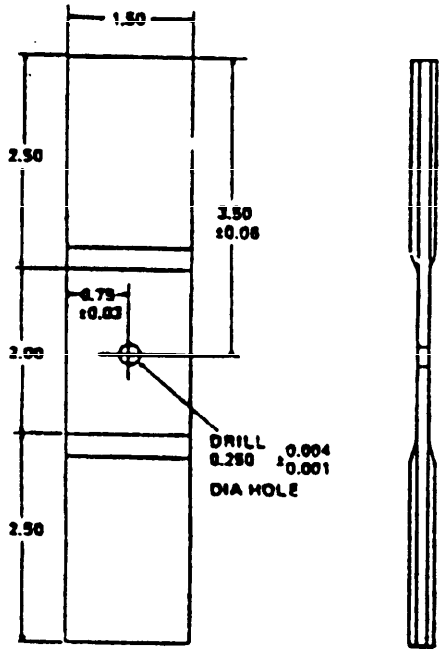

Drilled Hole

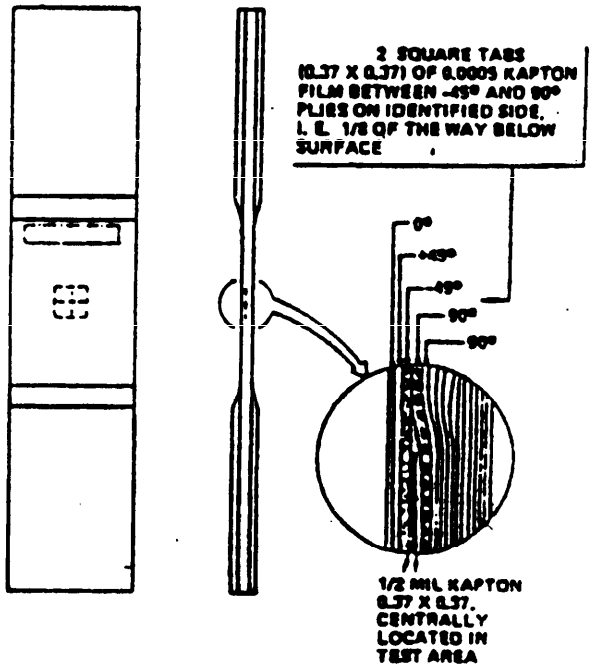

Embedded Film Patch

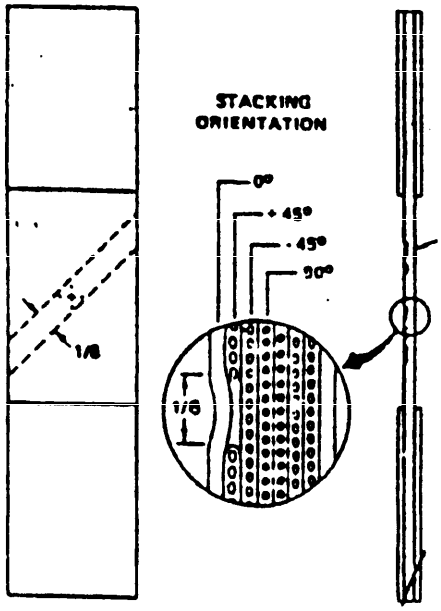

Ply Gap

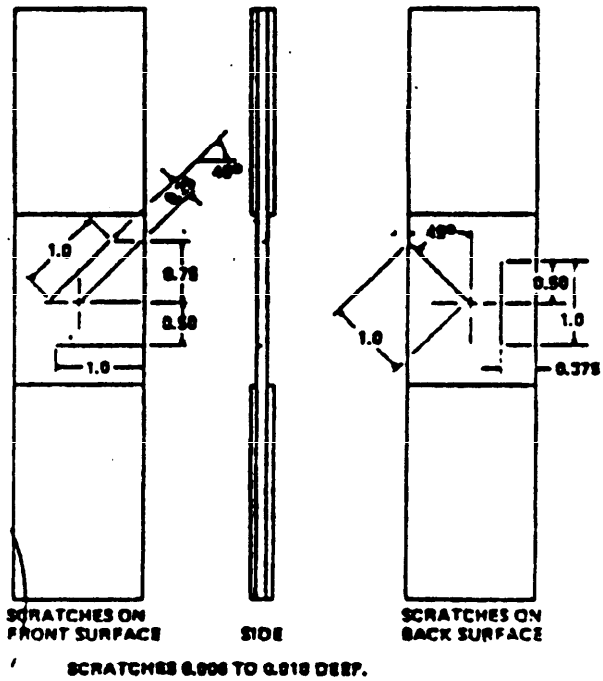

Surface Scratches

FIGURE 26. Fatigue coupons showing four different simulated flaws in a 16-ply graphite/epoxy composite. After Liber et al.(55)

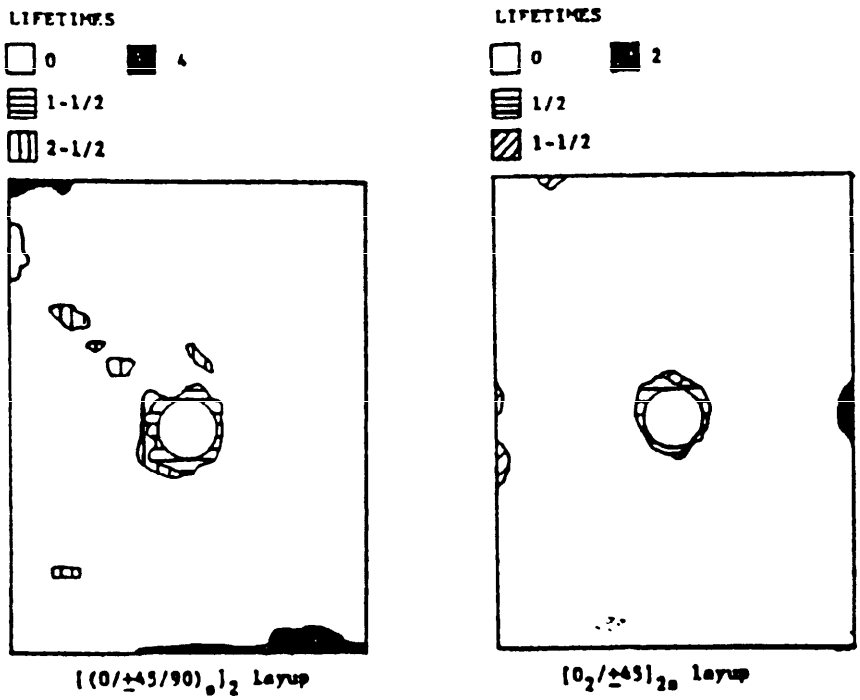

Drilled Hole

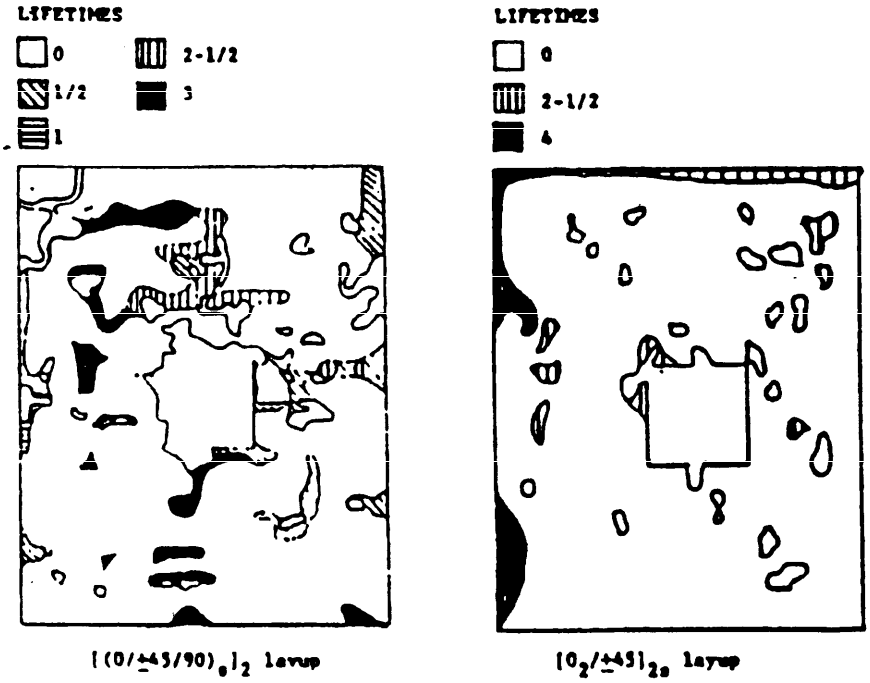

Embedded Film Patch

FIGURE 27. Contour C-Scan maps of flaw growth for flawed specimens indicated in figure 26. After Liber et al.(55)

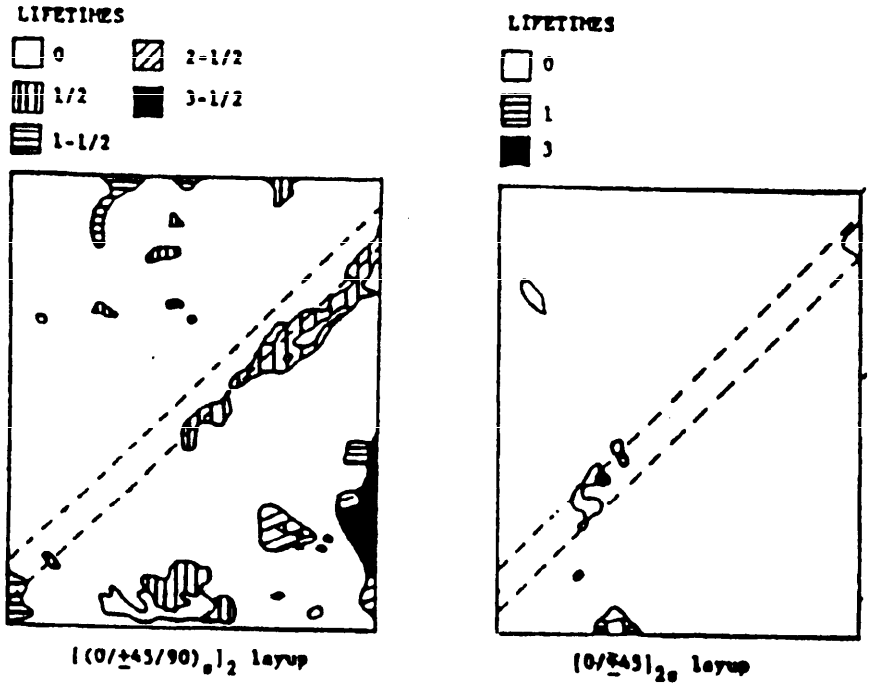

Ply Gap

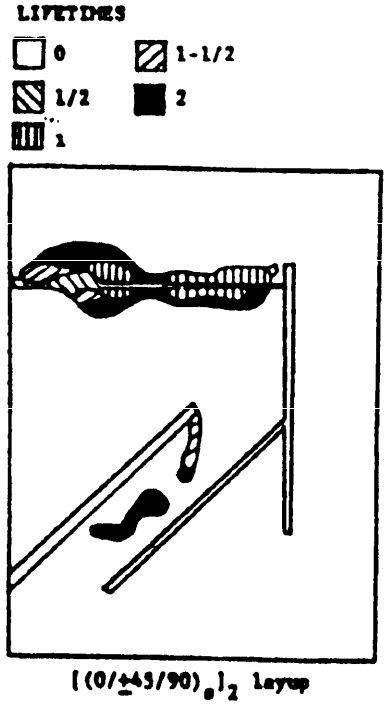

Surface Scratch

FIGURE 28. Contour C-Scan maps of flaw growth for flawed specimens indicated in figure 26. After Liber et al.(55)

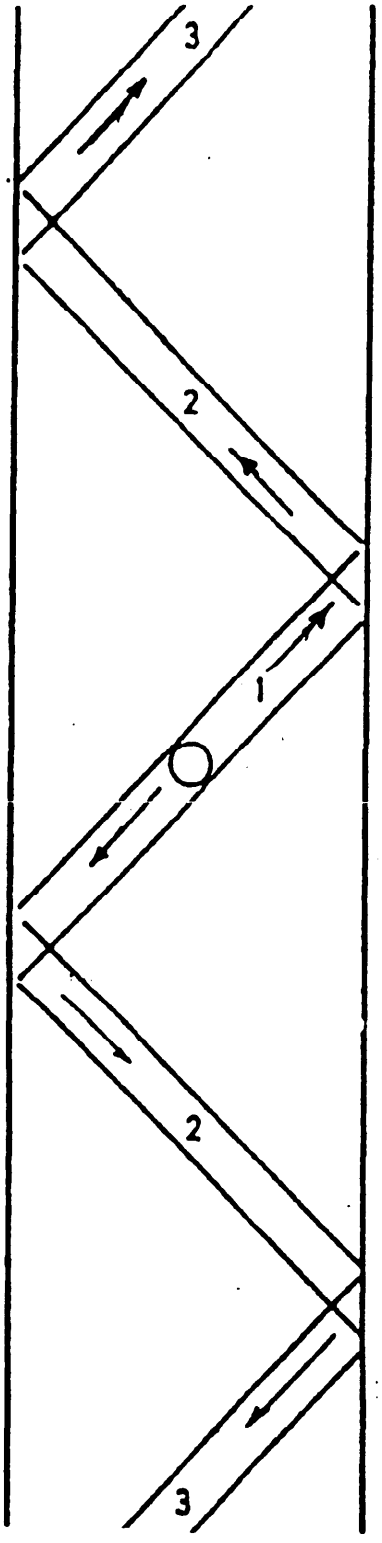

FIGURE 29. Propagation of disbonding along the +45 aligned fibers of the through hole simulated flaw.

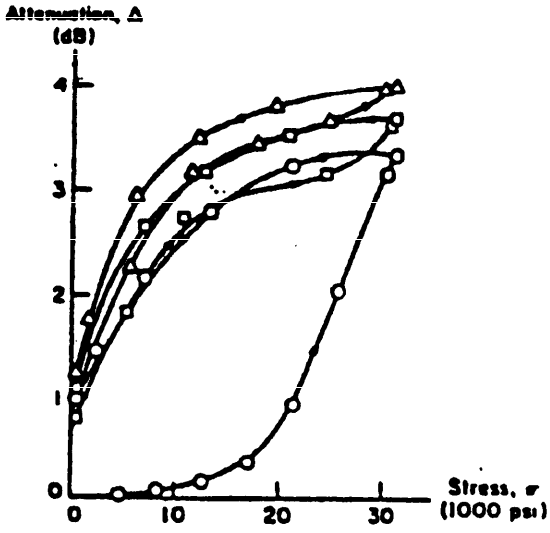

FIGURE 30. Attenuation response in a cross-ply specimen during cycling. Frequency of the ultrasound is 1 MHz. After Tauchert and Hsu.(39)

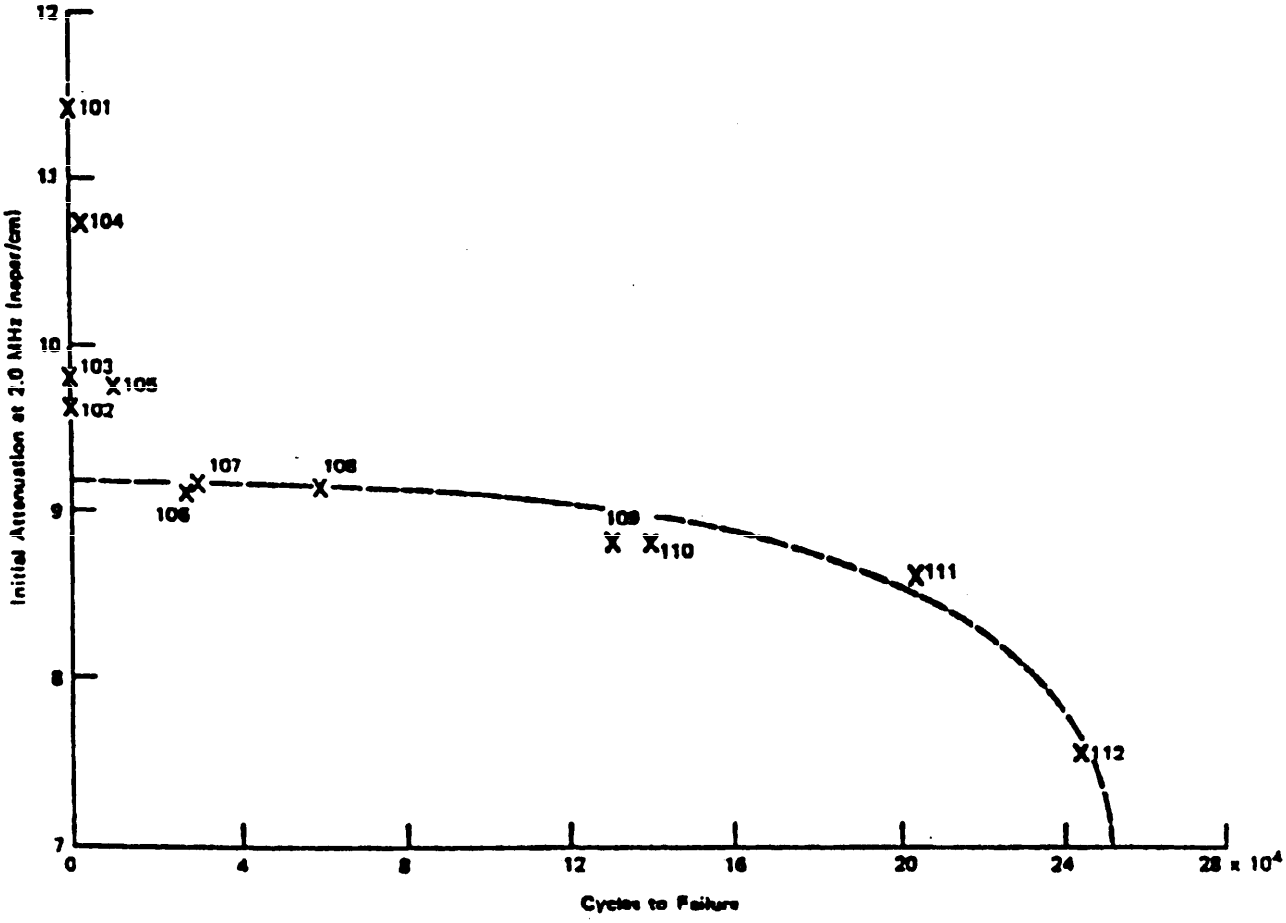

FIGURE 31. Initial attenuation at 2.0 MHz as function of the fatigue life. After Williams and Doll.(40)

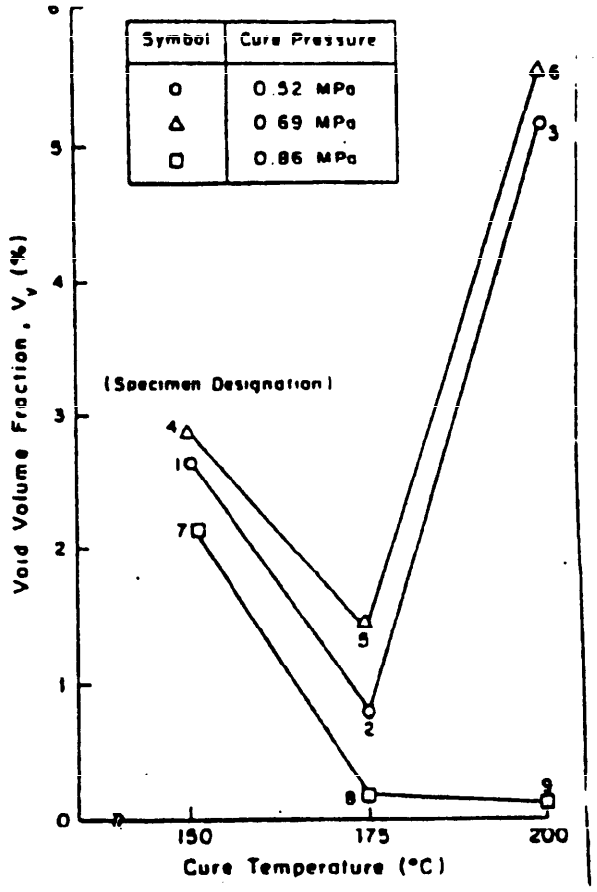

FIGURE 32. Composite void content for variations in cure temperature. After Williams, Yuce and Lee.(53)

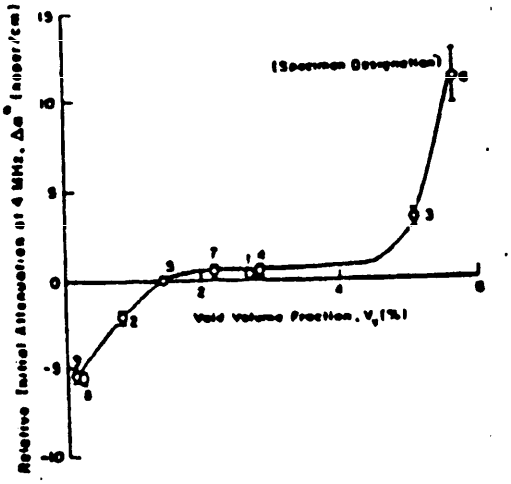

FIGURE 33. Initial attenuation-void content data. A frequency of 4 MHz was used for the attenuation measurements. After William, Yuce and Lee.(41)

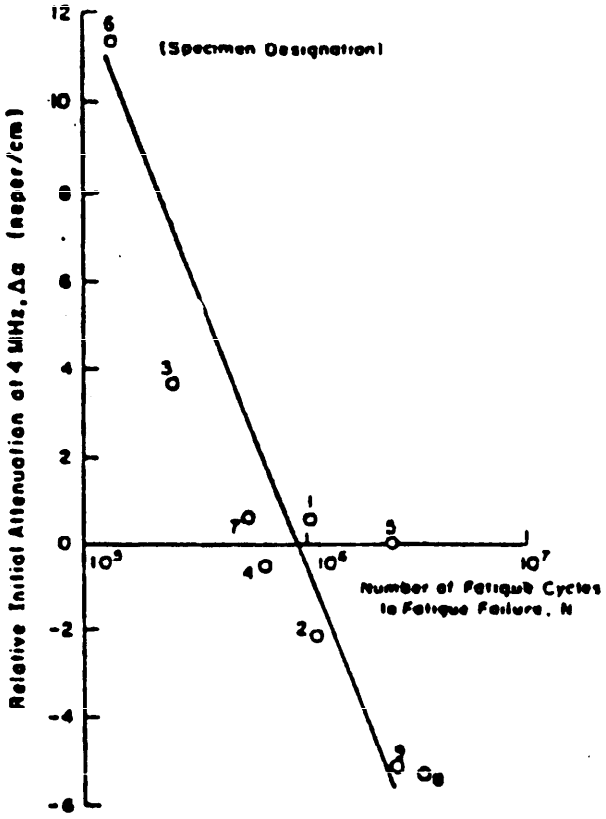

FIGURE 34. Relative attenuation at 4 MHz as a function of the number of fatigue cycles to failure. After Williams, Yuce and Lee.(41)

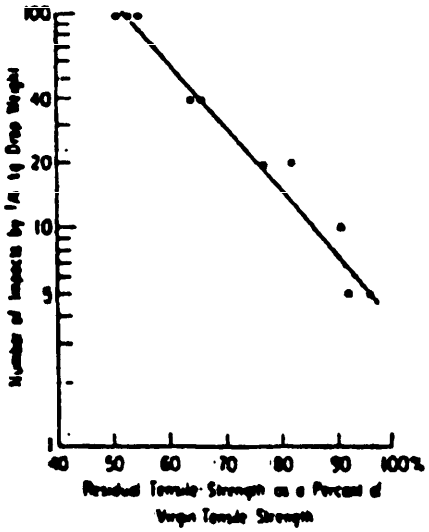

FIGURE 35. Impact damage as measured by the residual tensile strength. After Williams and Lampert.(25)

Vertical scale: 20V/Large Div.
Time sweep: 0.5μs/Large Div.

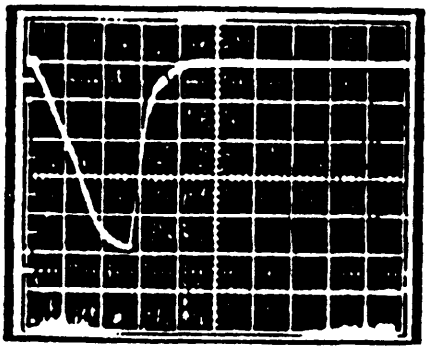

(a) Input Pulse

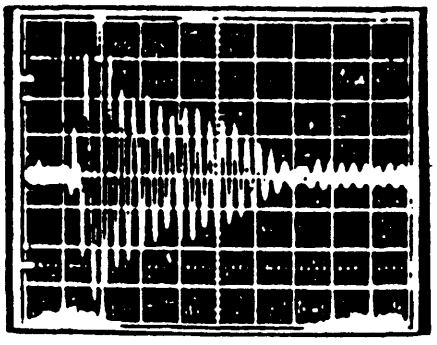

Vertical scales: 0.1V/Large Div.
Time sweeps: 10μs/Large Div.

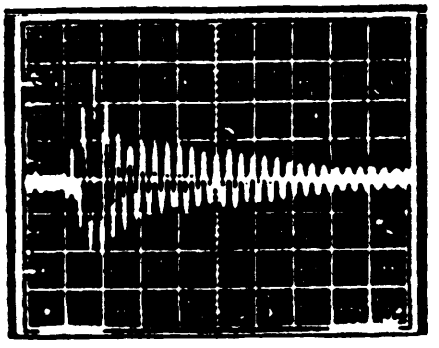

(b) Virgin Material

(c) After 100 Impacts

FIGURE 36. Typical pulses observed during stress wave factor determinations. After Vary and Lark.(56)

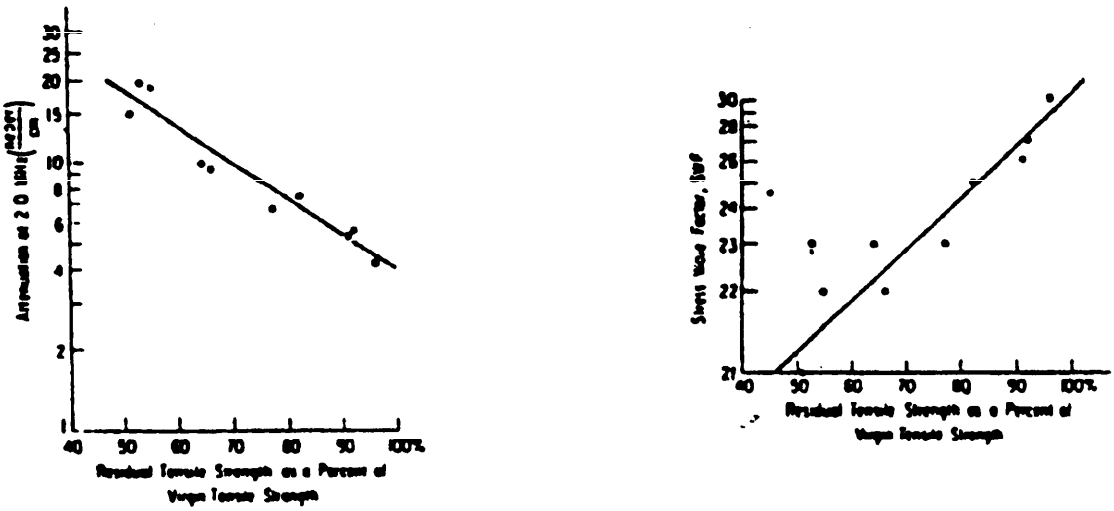

FIGURE 37. Ultrasonic indicators of impact damage. After Williams and Lampert.(25)

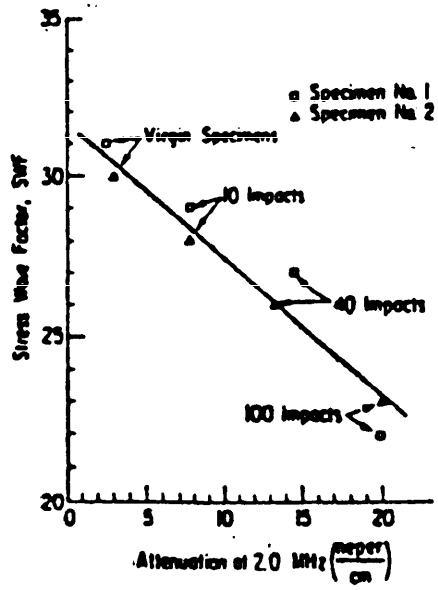

FIGURE 38. Comparison of the stress wave factor and through thickness attenuation to detect impact damage. After Williams and Lampert.(25)

of voids in the coupiant. The philosophy has often been to use a lot of

$$\begin{bmatrix} C_{11} & C_{12} & C_{13} & 0 & 0 & 0 \\ C_{12} & C_{22} & C_{23} & 0 & 0 & 0 \\ C_{13} & C_{23} & C_{33} & 0 & 0 & 0 \\ 0 & 0 & 0 & C_{44} & 0 & 0 \\ 0 & 0 & 0 & 0 & C_{55} & 0 \\ 0 & 0 & 0 & 0 & 0 & C_{66} \end{bmatrix}$$

(a)

$$\begin{bmatrix} C_{11} & C_{12} & C_{13} & 0 & 0 & 0 \\ C_{12} & C_{11} & C_{13} & 0 & 0 & 0 \\ C_{13} & C_{13} & C_{33} & 0 & 0 & 0 \\ 0 & 0 & 0 & C_{44} & 0 & 0 \\ 0 & 0 & 0 & 0 & C_{44} & 0 \\ 0 & 0 & 0 & 0 & 0 & \frac{C_{11}-C_{12}}{2} \end{bmatrix}$$

(b)

FIGURE 39. The stiffness matrices of the (a) orthotropic and (b) transverse isotropic structure.

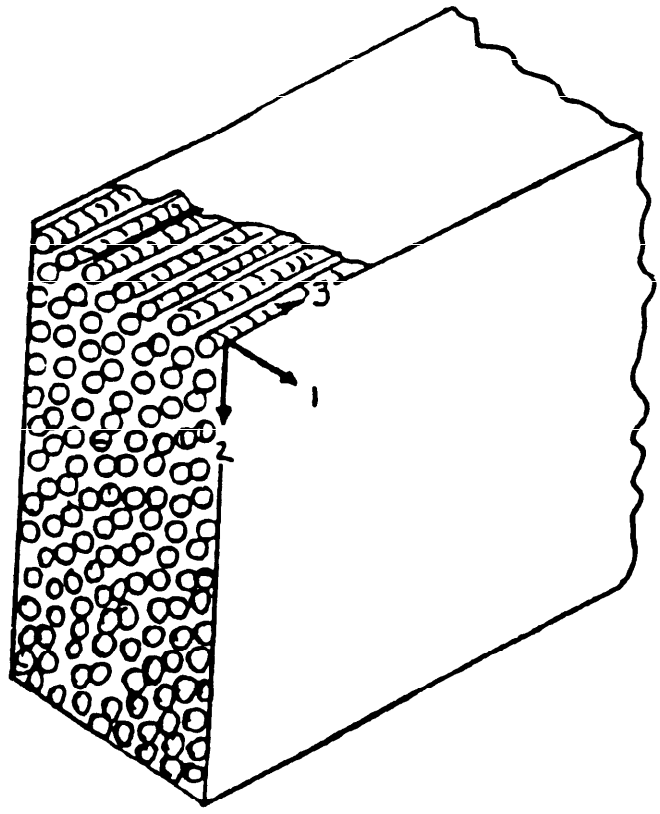

FIGURE 40. The transverse isotropic structure. The random array of the fibers is indicated.

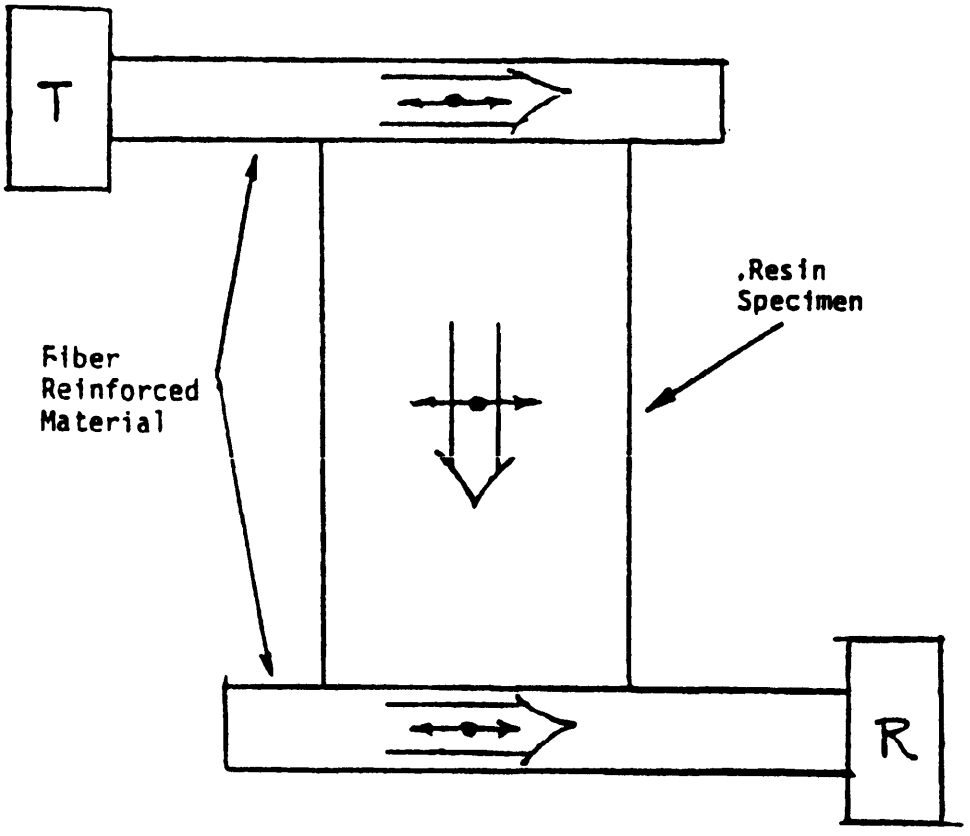

FIGURE 41. The longitudinal wave produced in the top unidirectional fiber reinforced material was converted to a shear wave at the top resin boundary and back again into a longitudinal wave at the lower resin boundary. This experimental arrangement was used to study the changes in the shear wave elastic constants as a function of the state of the cure. After Reynolds and Wilkinson.(45)

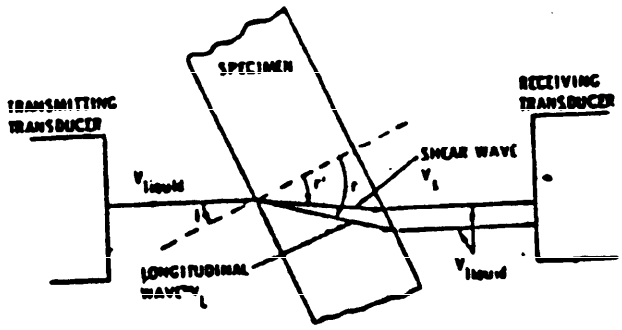

FIGURE 42. The immersion method apparatus for the measurement of elastic constants.

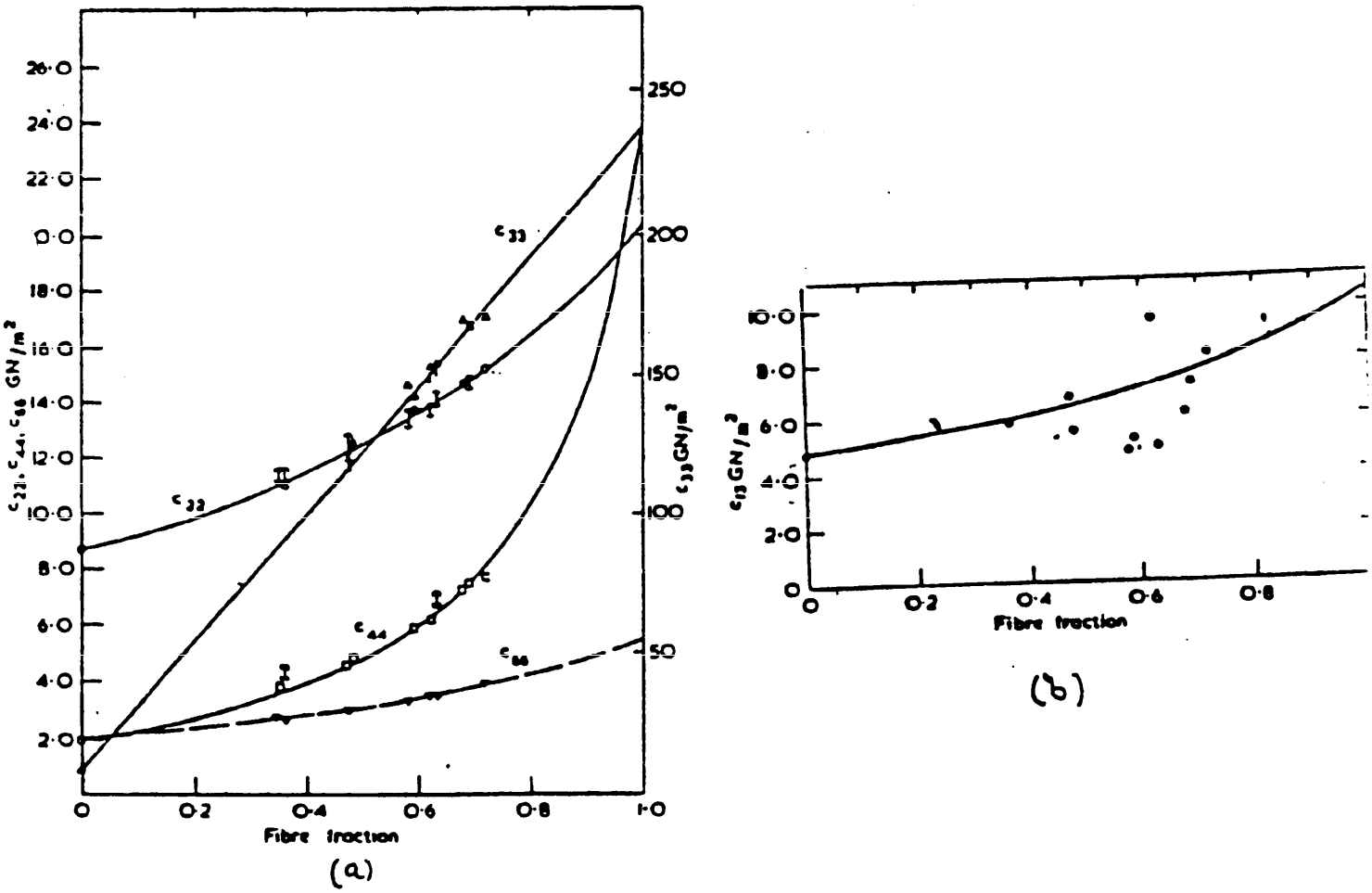

FIGURE 43. Experimental and theoreticalresults for the determination of the elastic constants of uniaxially aligned Modmor type II carbon fibers in Ciba LY558 epoxy resin. The theoretical (solid lines) are due to a theory proposed by Hashin and Rosen.(51) After Dean and Turner.(50)

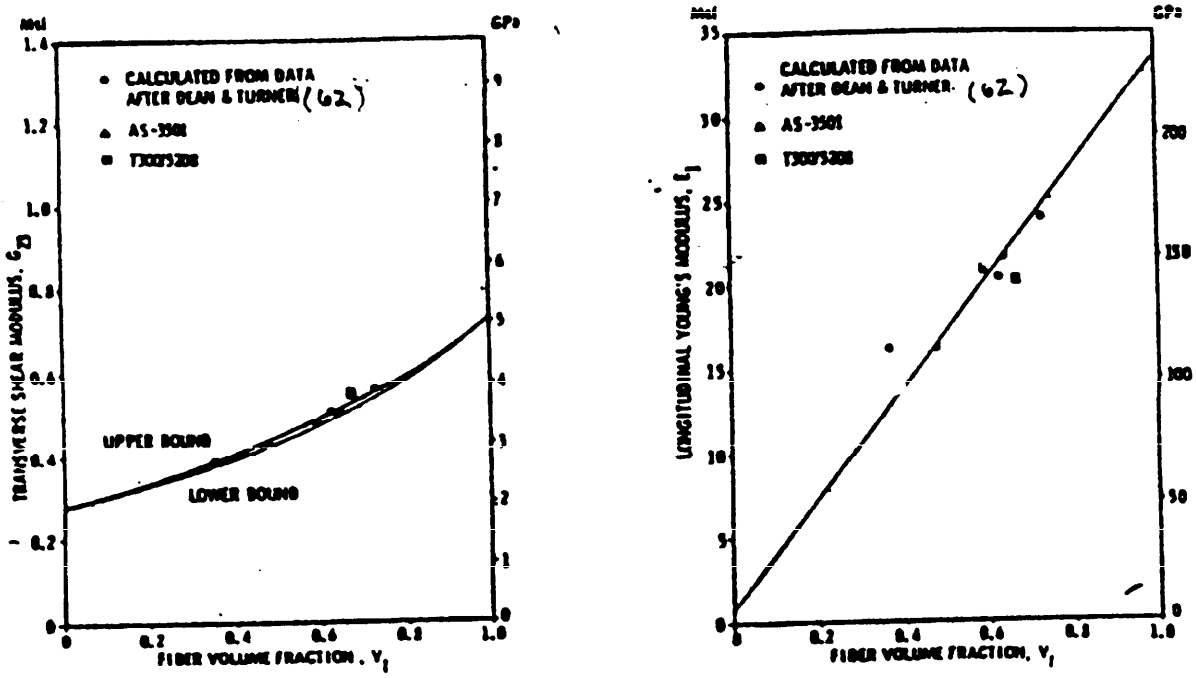

FIGURE 44. Engineering parameters derived from elastic constant measurements. After Kriz and Stinchcomt.(52)

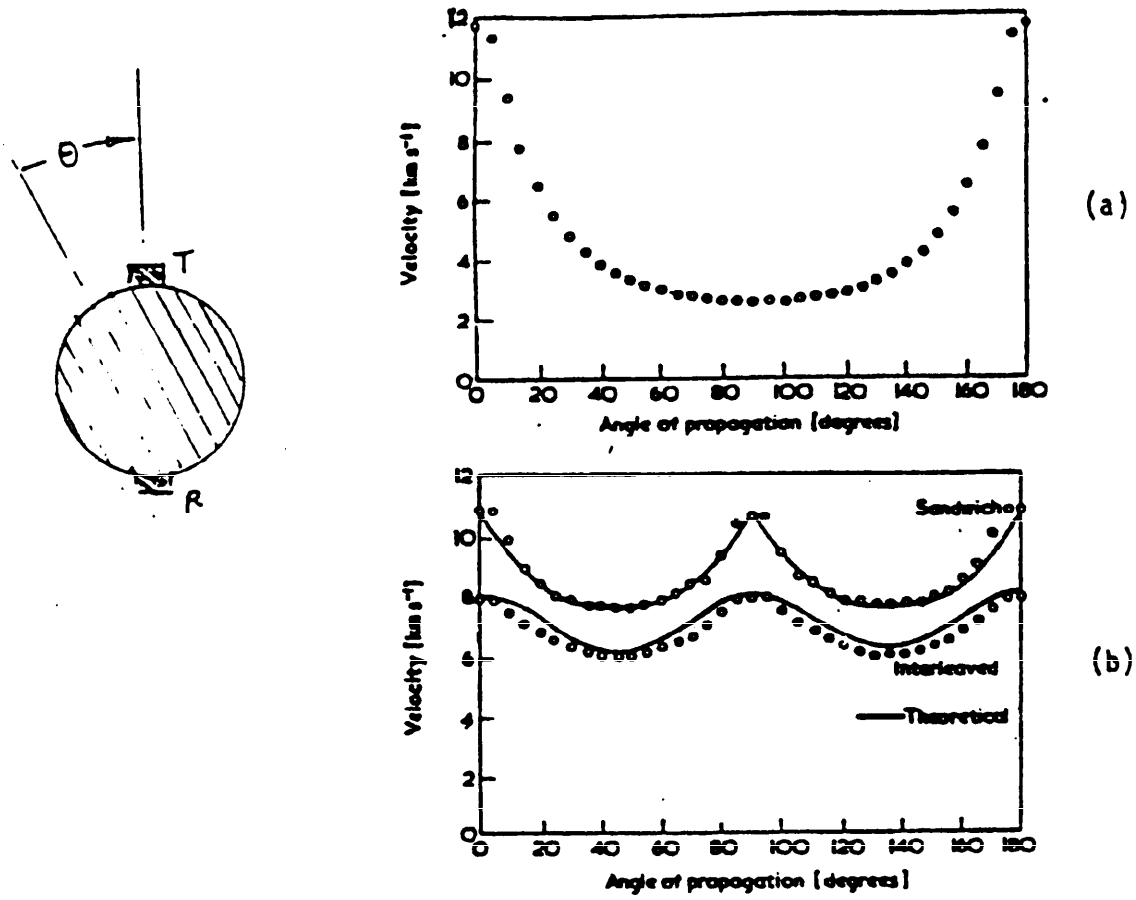

FIGURE 45. Longitudinal velocity within the plane of the fibers. After Reynolds and Wilkenson.(17)

REFERENCES

1. A. Vary and R.F. Lark, "Correlation of Fiber Composite Tensile Strength with the Ultrasonic Stress Wave Factor," NASA Lewis Research Center, Cleveland, Ohio, NASA TM-78846, April 1978.

2. D.E. W. Stone and B. Clarke, "Ultrasonic Attenuation as a Measure of Void Content in Carbon-Fibre Reinforced Plastics," Non-Destructive Testing, 137, June 1975.

3. R. Prakash and C.N. Owston, "Ultrasonic Determination of Lay-up Order in Cross-Plied CFRP." Composites 8(2): 100-102, April, 1977

4. Y. Bar-Cohen and R.L. Crane, "Acoustic-Backscattering of Subcritical Flaws in Composites," Mat. Eval., 40, 970, 1982.

5. E.J. Kohn, A.G. Sands and R.C. Clark, "Quantitative Measurement of Void Content in Glass Filament-Wound Composites and the correlation of Interlaminar Shear Strength With Vod Content," Ind. Eng. Chem. Prod. Res. Develop, 7(3), 179, 1968.

6. E.F. Olster, Chem. Abs. 78 30632, 1973.

7. Physics of Industrial Radiology, R. Halmshaw, Editor; American Elsevier Publishing Company, New York, 1966

8. N.C.W. Judd and W.W. Wright, "Voids and Their Effects on the Mechanical Properties of Composites - An Appraisal," SAMPE Journal, 14(1) January-February, 1978.

9. B.G. Martin, "Ultrasonic Attentuation Due to Voids in Fibre Reinforced Plastics," NDT International, 242 October 1976.

10. C.F. Ying and R. Truell, "Scattering of A Plane Longitudinal Wave By a Spherical Obstacle In An Isotropically Elastic Solid." J. Appl. Phys. 27, 1086, 1956.

11. R. Ziegler and R. Gertner, Giesserei, 45, 8, 185, 1958.

12. G.E. Lockyer, "Evaluation of A Resin - Ceramic Heat Shield Material By Ultrasonic Techniques," Mat. Eval. 23(3), 144, 1965.

13. S. Serabian, Presented at 1972 ASNT Meeting, Cleveland, Ohio, 1969.

14. R.H. Brockelman, "Evaluating Properties of Powder Iron Compact by Sonic Tests," Metal Progress, 95, July 1965.

15. M.J.P. Musgrave, Crystal Acoustics, Holden-Day, San Francisco, 1970.

16. B.G. Martin, "Ultrasonic Wave Propagation In Fiber-Reinforced Solids Containing Voids," J. Appl. Phys., 48(8), 3368, 1977.

17. W.N. Reynolds and S.J. Wilkinson, "The Propagation of Ultrasonic Waves In CFRP Laminates," J. Phys. D: Appl. Phys. 7, 50, 1974.

18. Hasin, Z., "On the Elastic Behavior of Fibre - Reinforced Materials of Arbitrary Transverse Phase Geometry," J. Applied Mech, 29, 143, 1962.

19. S. Boucher, "Effective Moduli of Quasi-Homogeneous Composite Materials (I) Infinitesimal Concentrations, Revue M Mec 21(3)(1975); II Finite Concentrations, Revue M Mech 22,(1)(1976). In French.

20. B.R. Jones and D.E.W. Stone, "Toward An Ultrasonic-Attenuation Technique to Measure Void Content in Carbon-Fibre Composites," Nondestructive Testing 9,(2), 71, 1976.

21. G.C. Knollman, D. Carver and J.J. Hartog, "Acoustic Imaging of Composites - The Ultrasonic Test That Requires No Interpretation," Mat. Eval., 36, 41, 1978.

22. P.H. Chang, W.G.W. Yee and J.C. Couchman, "Spectra Analysis Technique of Ultrasonic NDT of Advanced Composite Materials," Nondestructive Testing, 7(4), 194, 1974,

23. A. Vary and K.J. Bowles, "Use of An Ultrasonic - Acoustic Technique for Nondestructive Evaluation of Fiber Composite Strength," J. Testing and Evaluation, 7,(4), 185, ASTM, 1979.

24. J.M. Rodgers, "Inspection of Composites and Adhesive-Bonded Structures by the Acousto-Ultrasonic Method," Presented at the Air Transport Association-Nondestructive Testing Forum, Atlanta, Georgia, September 1982.

25. J.H. Williams, Jr. and N.R. Lampert, "Ultrasonic Evaluation of Impact-Damaged Graphite Fiber Composites," Materials Evaluation, 38,(12), 68, 1980.

26. D.T. Hayford and E.G. Henneke, "A Model For Correlating Damage and Ultrasonic Attenuation in Composites" Composite Materials: Testing and Design (Fifth Conference), ASTM STP 674, S.W Tsai, Editor; 1979.

27. K.L. Reifsnider, E.G. Henneke II and W.W. Stinchcomb, "Defect Property Relationships in Composite Materials," Technical Report AFML-TR-76-81, Part I (April 1976) and Part II (June 1977), AFML Contract No. F33165-75-C-5119.

28. D.T. Hayford, E.G. Henneke, and W.W. Stinchcomb, "The Correlation of Ultrasonic Attenuation and Shear Strength in Graphite-Polyimide Composites," J. Composite Materials, 11, 429, 1977.

29. M.J. Salkind, Applications in Composite Materials, ASTM, STP524, 1973.

30. J.B. Sturgeon, "Fatigue Mechanisms, Characterization of Defects and Their Detection in Reinforced Plastic Materials," British J. of NDT, Nov. 1978.

31. J.J. Nevadunski, J.J. Lucas, M.J. Salkind, "Early Fatigue Damage Detection in Composite Materials," J. Composite Materials, 9, 394, 1975.

32. K.L. Reifsnider, W.W. Stinchcomb, R.S. Williams and L.A. Marcus, "Heat Generation in Composite Materials During Fatigue Loading," VPI, AFOSR-TR-73-1961, May 1973.

33. K.L. Reifsnider, "Fatigue in Composite Materials," AGARD Report 638, 1976.

34. R.S. Williams and K.L. Reifsnider, "Investigation of Acoustic Emission During Fatigue Loading of Composite Specimens" J. Composite Materials 8, 340, 1974.

35. G.L. Roderick and J.D. Whitcomb, "X-Ray Method Shows Fibers Fail During Fatigue of Boron-Epoxy Laminates" J. Composite Materials 9, 391, 1975.

36. E.G. Henneke, W.W. Stinchcomb, and K.L. Reifsnider, "Some Ultrasonic Methods for Characterizing Response of Composite Materials," First International Symposium on Ultrasonic Material Characterization. National Bureau of Standards, Gaithersburg, MD, June 1978

37. T. Liber, I.M. Daniel and S.W. Schramm "Ultrasonic Techniques for Inspecting Flat and Cylindrical Composite Specimens," Nondestructive Evaluation and Flaw Criticality for Composite Materials, ASTM, R.B. Pipes, Editor, Oct. 1978.

38. R. Truell and A. Hikata, "Fatigue and Ultrasonic Attenuation," ASTM Symposium On Nondestructive Testing, 1957.

39. T.R. Tauchert and N.N. Hsu, "Influence of Stress Upon Internal Damping In A Fiber Reinforced Composite Material," J. Composite Materials, 7, 516, 1973.

40. J.H. Williams, Jr., and B. Doll, "Ultrasonic Attenuation As An Indicator of Fatigue Life of Graphite Fiber Epoxy Composite," Mat. Eval. 38(5), 33, 1980.

41. J.H. Williams, Jr., H. Yuce and S.S. Lee, "Ultrasonic and Mechanical Characterization of Fatigue States of Graphite Epoxy Composite Laminates," Mat. Eval. 40, 560, 1982.

42. H.B. Huntington, "The Elastic Constants of Crystals," Solid State Physics, 7, Academic Press, New York, 1958.

43. J.E. Zimmer and J.R. Cost, "Determination of the Elastic Constants of a Unidirectional Fiber Composite Using Ultrasonic Velocity Measurements," J. Acoust. Soc. Am., 47,(3), 795, 1970.

44. J.R. Neighbors, "An Approximate Method for Determination of the Elastic Constants of Single Crystals." JASA 26, 865, 1954.

45. L. Gold, "Compilation of Velocity Data For Cubic and Hexagonal Metals, J. Appl. Phys., 21, 541, 1950.

46. W. Sache, "Measurement of the Elastic Moduli of Continuous-Filament and Eutectic Composite Materials," J. Composite Mater. B, 379, 1974.

47. J.H. Gieske and R.E. Allred, "Elastic Constans of B-Al Composites By Ultrasonic Velociy Measurements." Experimental Mechanics 14(4):158-165, April 1974

48. J.R. Assay, S.R. Urzendowski and A.H. Guenther, "Ultrasonic and Thermal Studies of Selected Plastics, Laminated Materials and Metals," Air Force Weapons Laboratory Report (AFWL-TR-67-91), Alburqueque, NM., 1967.

49. M.F. Markham, "Measurement of Elastic Constants of Fiber Composites by Ultrasonics," Composites, 1, 145, 1970.

50. G.D. Dean and P. Turner, "The Elastic Properties of Carbon Fibres and Their Composites." Composites 4(4): 174-180, July 1973.

51. Z. Hashin and B.W. Rosen, "The Elastic Moduli of Fiber-Reinforced Materials," J. of Applied Mechanics, 31(1), 1964.

52. R.D. Kriz and W.W. Stinchcomb, "Elastic Moduli of Transversely Isotropic Graphite Fibers and Their Composites," Experimental Mechanics, 41, February, 1979.

53. Z. Harshin, "Theory of fiber Reinforced Materials," NASA-CR-1974.

54. R.M. Jones, Mechanics of Composite Materials, McGraw-Hill Book Company, NYC, 1975.

55. T. Liber, T.M. Daniel and S.W. Schramm, "Ultrasonic Techniques For Inspecting Flat and Cylindrical Composite Specimens," Nondestructive Evaluation and Flaw Criticality for Composite Materials, ASTM, R.B. Pipes, Editor, Oct. 1978.

56. A Vary and R.F. Lark, "Correlation of Fiber Composite Tensile Strength With The Ultrasonic Stress Wave Factor," J. Testing and Evaluation, NASA TM-78846 (1978).

57. B.D. Agarwal and L.J. Broutman, Analysis and Performance of Fiber Composites, J. Wiley & Sons, New York, 1980.

Custodians:
Army - MR
Navy - AS
Air Force - 20

Review activities:
Army - MI, AV, AT, AR
Navy - OS
Air Force - 99, 84, 82, 80

User activities:
Army - ME
Navy - SH

Military Coordinating Activity
Army - MR

Project NDTI-0154

WP# ID-0205B/DISC-0168B. FOR MTL USE ONLY.

INSTRUCTIONS: In a continuing effort to make our standardization documents better, the DoD provides this form for use in submitting comments and suggestions for improvements. All users of military standardization documents are invited to provide suggestions. This form may be detached, folded along the lines indicated, taped along the loose edge *(DO NOT STAPLE)*, and mailed. In block 5, be as specific as possible about particular problem areas such as wording which required interpretation, was too rigid, restrictive, loose, ambiguous, or was incompatible, and give proposed wording changes which would alleviate the problems. Enter in block 6 any remarks not related to a specific paragraph of the document. If block 7 is filled out, an acknowledgement will be mailed to you within 30 days to let you know that your comments were received and are being considered.

NOTE: This form may not be used to request copies of documents, nor to request waivers, deviations, or clarification of specification requirements on current contracts. Comments submitted on this form do not constitute or imply authorization to waive any portion of the referenced document*(s)* or to amend contractual requirements.

(Fold along this line)

(Fold along this line)

DEPARTMENT OF THE ARMY

NO POSTAGE NECESSARY IF MAILED IN THE UNITED STATES

OFFICIAL BUSINESS
PENALTY FOR PRIVATE USE $300

BUSINESS REPLY MAIL
FIRST CLASS PERMIT NO. 12062 WASHINGTON D. C.
POSTAGE WILL BE PAID BY THE DEPARTMENT OF THE ARMY

Director
US Army Laboratory Command
Materials Technology Laboratory
ATTN: SLCMT-MSE
Watertown, Ma. 02171-0001

STANDARDIZATION DOCUMENT IMPROVEMENT PROPOSAL

(See Instructions – Reverse Side)

1. DOCUMENT NUMBER	2. DOCUMENT TITLE

3a. NAME OF SUBMITTING ORGANIZATION	4. TYPE OF ORGANIZATION *(Mark one)*
	☐ VENDOR
b. ADDRESS *(Street, City, State, ZIP Code)*	☐ USER
	☐ MANUFACTURER
	☐ OTHER *(Specify)*:

5. PROBLEM AREAS

a. Paragraph Number and Wording:

b. Recommended Wording:

c. Reason/Rationale for Recommendation:

6. REMARKS

7a. NAME OF SUBMITTER *(Last, First, MI)* – Optional	b. WORK TELEPHONE NUMBER *(Include Area Code)* – Optional
c. MAILING ADDRESS *(Street, City, State, ZIP Code)* – Optional	8. DATE OF SUBMISSION *(YYMMDD)*

(TO DETACH THIS FORM, CUT ALONG THIS LINE.)

DD FORM 82 MAR 1426

PREVIOUS EDITION IS OBSOLETE.